J Neurophysiol 113: 1727–1742, 2015.
First published December 17, 2014; doi:10.1152/jn.00420.2014.

Tracking the evolution of crossmodal plasticity and visual functions before and after sight restoration

Giulia Dormal,[1,2] Franco Lepore,[1] Mona Harissi-Dagher,[3] Geneviève Albouy,[4] Armando Bertone,[5] Bruno Rossion,[2] and Olivier Collignon[1,6]

[1]*Centre de Recherche en Neuropsychologie et Cognition (CERNEC), Université de Montréal, Montreal, Quebec, Canada;* [2]*Institute of Research in Psychology (IPSY), Center for Cognitive and Systems Neuroscience, Université catholique de Louvain, Louvain-la-Neuve, Belgium;* [3]*Department of Ophthalmology, Centre Hospitalier de l'Université de Montréal (CHUM) Notre Dame, Montreal, Quebec, Canada;* [4]*Centre de recherche de l'Institut Universitaire de Gériatrie de l'Université de Montréal (CRIUGM), Montreal, Quebec, Canada;* [5]*Department of Education and Counselling Psychology, McGill University, Montreal, Quebec, Canada; and* [6]*Centro Interdipartimentale Mente/Cervello (CIMeC), Università di Trento, Mattarello, Italy*

Submitted 8 June 2014; accepted in final form 15 December 2014

Dormal G, Lepore F, Harissi-Dagher M, Albouy G, Bertone A, Rossion B, Collignon O. Tracking the evolution of crossmodal plasticity and visual functions before and after sight restoration. *J Neurophysiol* 113: 1727–1742, 2015. First published December 17, 2014; doi:10.1152/jn.00420.2014.—Visual deprivation leads to massive reorganization in both the structure and function of the occipital cortex, raising crucial challenges for sight restoration. We tracked the behavioral, structural, and neurofunctional changes occurring in an early and severely visually impaired patient before and 1.5 and 7 mo after sight restoration with magnetic resonance imaging. Robust presurgical auditory responses were found in occipital cortex despite residual preoperative vision. In primary visual cortex, crossmodal auditory responses overlapped with visual responses and remained elevated even 7 mo after surgery. However, these crossmodal responses decreased in extrastriate occipital regions after surgery, together with improved behavioral vision and with increases in both gray matter density and neural activation in low-level visual regions. Selective responses in high-level visual regions involved in motion and face processing were observable even before surgery and did not evolve after surgery. Taken together, these findings demonstrate that structural and functional reorganization of occipital regions are present in an individual with a long-standing history of severe visual impairment and that such reorganizations can be partially reversed by visual restoration in adulthood.

blindness; crossmodal plasticity; sight recovery; ventral-dorsal pathways

ONE OF THE MOST STRIKING EXAMPLES of experience-dependent brain plasticity originates from studies of blind individuals, whose cortical areas normally devoted to vision reorganize to support nonvisual sensory and cognitive functions (Bavelier and Neville 2002; Noppeney 2007). Crossmodal plasticity is thought to be functionally relevant since *1*) its strength may correlate with superior abilities in the remaining senses in early blind individuals (Amedi et al. 2003; Gougoux et al. 2005); *2*) transcranial magnetic stimulation (TMS) targeting the occipital cortex of early blind individuals has a detrimental effect on nonvisual performance (Amedi et al. 2004; Cohen et al. 1997; Collignon et al. 2007); and *3*) crossmodal recruitment of occipital regions in early blind individuals seems to retain the typical functional specialization of these cortical regions (Collignon et al. 2011b; Reich et al. 2011; for reviews see Dormal and Collignon 2011; Ricciardi and Pietrini 2011).

Functional crossmodal plasticity inevitably raises important challenges for individuals undergoing surgical procedures to recover vision, as the deprived and reorganized occipital cortex may not provide the necessary cortical resources for adequate visual analysis of the restored optical input (Collignon et al. 2011a; Merabet and Pascual-Leone 2009). Support for this assumption comes from research conducted on deaf individuals demonstrating that the success of cochlear implants is inversely related to the amount of crossmodal visual activity measured in the auditory cortex prior to implantation (Buckley and Tobey 2011; Lee et al. 2007; Sandmann et al. 2012; Strelnikov et al. 2013; but see Heimler et al. 2014 for a critical review).

Empirical investigations of this question in visually deprived individuals are scarce. Cases of sight recovery in adulthood after long-standing blindness typically encounter severe and permanent visual deficits even years after the intervention [Ackroyd et al. 1974; Carlson et al. 1986; Fine et al. 2003; Gregory and Wallace 1974 (original work published in 1963)]. To date, only one functional magnetic resonance imaging (fMRI) study has jointly investigated visual- and auditory-driven responses in the occipital cortex of two sight recovery individuals (Saenz et al. 2008). In these subjects, crossmodal auditory motion responses coexisted with visual motion responses in area MT+/V5. Since this study was carried out several years after sight restoration, no observations were reported about the evolution of occipital functions before and after sight was regained.

Most cases of vision loss occur gradually, and individuals often maintain some degree of residual vision (Merabet and Pascual-Leone 2009). Surprisingly, the question of whether crossmodal plasticity may be observed even in cases where the sensory deprivation is not total remains largely unexplored. This is an issue of particular relevance considering that these individuals are the main targets of new advances in surgical procedures to restore vision (Aldave et al. 2009; Robert and Harissi-Dagher 2011).

Here we provide the first extensive longitudinal investigation of a case of sight recovery after a life-long history of severe visual impairment. We performed both pre- and post-

Address for reprint requests and other correspondence: O. Collignon, Via delle Regole 101, 38060 Mattarello (TN), Italy (e-mail: olivier.collignon@unitn.it).

surgery measurements and combined behavioral, neurostructural (MRI), and neurofunctional (fMRI) methods. Our goals were threefold. First, we aimed to investigate the presence of crossmodal plasticity prior to surgery despite (poor) residual vision. Second, we aimed to track the evolution of such putative crossmodal plasticity after surgery, in order to test whether it may decrease or disappear as a result of visual recovery. Third, we investigated the integrity of the ventral and the dorsal visual pathways before surgery and their evolution after optical quality improvement.

MATERIALS AND METHODS

Case Description

KL is a right-handed woman, born in 1965 in Meteghan, Nova Scotia, Canada. Her visual impairment history was assessed by obtaining access to her medical records, by discussing the case with the ophthalmologist who carried out the ophthalmic procedure (M. Harissi-Dagher), and by carrying out detailed anamneses with her and with her 9-yr-older brother. KL's vision has been highly altered since very early in life. At 10 mo of age, her parents and older brothers noticed a lack of visually guided behavior and an inability to avoid obstacles around her. She was diagnosed between 2 and 3 yr of age with dense bilateral cataracts, which were surgically removed at that time by extraction of the crystalline lens bilaterally. The surgery was not successful in restoring functional vision, since KL has only experienced residual patterned color and motion information in the right eye and none in the left. The left eye was deemed amblyopic. During infancy and adolescence, she attended school in specific classes for children with learning disabilities. At that time, she would always sit a few feet away from the blackboard and was capable of reading books with large letters from a distance of ~5 in. She had to stop attending school in grade 8 (first year of high school), as there were no more adapted classes and her vision was too altered to allow her to attend regular classes. At home she would rather listen to music than watch television, and when she did watch television it was from ~3 in. from the screen. She never played any sports involving a ball as she was unable to see the ball in time in order to catch it. KL and her older brother recall that it was never possible for her to recognize anyone familiar solely based on their face.

KL got married and moved from Nova Scotia to Quebec in 1984. In 1996, rhegmatogenous retinal detachment occurred in her right eye for which she underwent surgical repair by pars plana vitrectomy. In 2000, a rhegmatogenous retinal detachment occurred again in the same eye, which was also repaired by pars plana vitrectomy. She worked between 1995 and 2007, until her vision further decreased to a point where she stopped working. Because of her cataract surgery at a young age, the cornea of both eyes became edematous. Corneal grafting was thus necessary to attempt to improve the visual acuity lost because of bullous keratopathy. A corneal graft was attempted in her right eye in December 2008, and an anterior chamber lens was implanted to correct the refractive power. The corneal graft was rejected in September 2010. A second corneal graft was attempted in October 2010 and was rejected again 3 mo later. At that point, visual acuity in her medical records was reported to be 20/300 and KL resorted to using a white cane. A Boston keratoprosthesis was implanted in her right eye in April 2012. A soft contact lens with optical correction of −0.5 diopters was placed to protect the eye. KL was tested with this correction at 1.5 mo after keratoprosthesis. In August 2012, the optical correction of the lens was increased to −6 diopters to improve distance vision, and KL was prescribed glasses with optical correction of +2 diopters for near vision. She was tested with this correction at 7 mo after keratoprosthesis.

General Experimental Design and Control Participants

KL was tested in three separate sessions involving identical behavioral, MRI, and fMRI procedures. The first session, hereafter referred to as Pre, took place 3 wk (18 days) prior to surgery. The two other sessions, hereafter referred to as Post 1.5m and Post 7m, took place 1.5 mo (48 days) and 7 mo (218 days) after visual restoration with Boston keratoprosthesis (Khan et al. 2007). Behavioral tasks consisted of computerized tests evaluating visual acuity, contrast sensitivity, global motion detection, face/nonface categorization, and individual face discrimination. Each neuroimaging session comprised four functional runs followed by the acquisition of a high-resolution anatomical image to investigate structural changes across time. Functional runs consisted of a motion localizer, a face localizer, and two auditory experiments. Three normally sighted right-handed women with corrected-to-normal vision aged 55, 40, and 52 yr were tested in the behavioral experiments and served as control participants (sighted control subjects). For MRI measures, we used previously acquired anatomical images from nine normally sighted subjects who were scanned on two occasions separated by a delay that ranged between 35 days and 3.5 yr (mean ± SD delay = 1.45 ± 1.32 yr; mean ± SD age at *scan 1* = 35 ± 10 yr; mean ± SD age at *scan 2* = 36 ± 10 yr; 3 women, 6 men). For fMRI experiments, we used previously acquired data with identical paradigms from 12 sighted control subjects with normal or corrected-to-normal vision for the motion localizer, the face localizer, and *auditory experiment 1* (4 women, 8 men; mean ± SD age = 29 ± 4.3 yr) and from 17 sighted control subjects with normal or corrected-to-normal vision (9 women, 8 men; mean ± SD age = 40 ± 14 yr), 12 early blind individuals (4 women, 8 men; mean ± SD age = 41 ± 11 yr), and 10 late blind individuals (8 women, 2 men; mean ± SD age = 48 ± 11 yr) for *auditory experiment 2* (see Collignon et al. 2011b, 2013). All participants gave their written informed consent to take part in the study, which was approved by the research ethic and scientific boards of the Quebec Bio-Imaging Network (QBIN), the Notre-Dame Hospital (CHUM), and the Centre for Interdisciplinary Research in Rehabilitation of Greater Montreal (CRIR).

Behavioral Experiments

Behavioral tasks consisted of computerized tests evaluating distance visual acuity, contrast sensitivity function, global motion detection thresholds, face/nonface categorization, and face individuation abilities. The tasks were administered in a dimly lit room and presented on a Viewsonic (PT775) CRT monitor (330 mm × 245 mm). Stimulus generation, presentation, and data collection for tests of distance visual acuity, contrast sensitivity, and global motion detection were controlled by a Macintosh Pro 2.8 GHz Quad-Core Intel Xeon using the DataPixx (www.vpixx.com) graphic program and visual stimulator [16-bit video digital-to-analog converter (DAC)]. The mean luminance of the display was 50.0 cd/m^2 [x = 0.2783, y = 0.3210 in CIE (Commission Internationale de l'Eclairage) u', v' color space], where L_{min} and L_{max} were 0.5 and 99.50 cd/m^2, respectively. Screen resolution was 1,280 × 1,024 pixels, and refresh rate was 85 Hz. Stimulus presentation and data collection for the face/nonface categorization and the face individuation tasks were controlled with an HP Compaq dc5850 Microtower PC using E-prime2 (Psychology Software Tools). Screen resolution was 1,024 × 768 pixels, and refresh rate was 60 Hz.

Distance visual acuity. Distance visual acuity was measured binocularly and monocularly with a Landolt-C paradigm at a distance of 285 cm from the computer screen (with the exception of KL at Pre, who was tested at 100 cm because of her inability to carry out the task at the same distance). Stimuli corresponded to high-contrast white optotypes ($L_{optotype}$ = 99.5 cd/m^2) on a black background ($L_{background}$ = 0.5 cd/m^2). Participants were asked to identify the orientation (up, down, left, or right) of the gap opening of the optotype using a four-alternative forced-choice paradigm (4AFC). Far visual acuity was

defined by Snellen decimal acuity, the reciprocal of the smallest resolvable visual angle of the optotype gap in arc minutes needed to correctly identify its orientation.

Contrast sensitivity. Contrast sensitivity function (CSF) was assessed binocularly at a distance of 57 cm from the computer screen by measuring contrast detection thresholds to luminance-defined vertically oriented sine-wave gratings with smoothed edges (in Gaussian envelope). Grating size was 20° × 20° when viewed from 57 cm. The mean luminance of the remainder of the display was 50 cd/m^2. Detection thresholds were measured separately for gratings of 0.25, 0.5, 1, 2, 4, 6, and 8 cycles per degree (cpd). In each trial, the target grating appeared in either one of two successively presented frames of 1-s duration each and separated by a 200-ms interval. A sound was emitted concomitantly with each frame presentation. Participants were instructed to indicate whether the target grating was present in the first or the second frame. CSF was calculated for each participant using the inverse of the contrast detection threshold measured for each spatial frequency.

Global motion detection. Global motion detection thresholds were measured separately for radial and vertical trajectories at a distance of 57 cm from the computer screen. Stimuli consisted of limited-lifetime random-dot kinematogram displays (RDKs) (Newsome and Paré 1988). One hundred white dots (0.75° diameter, L_{dots} = 99.5 cd/m^2) with a limited lifetime of 250 ms were presented against a 23° × 23° black background square ($L_{background}$ = 0.5 cd/m^2) and moved at a speed of 12°/s. A subset of randomly chosen (signal) dots moved in the same direction, whereas the remaining (noise) dots in the display moved in random directions. Signal strength was manipulated by varying the percentage of signal dots in the display. In the radial task, signal dots moved toward (contracting) or away from (expanding) the center of the screen. In the vertical task, signal dots moved upward or downward. Participants were instructed to identify the direction of the signal dots. We measured a coherence threshold for each of the two tasks (i.e., minimum percentage of signal dots required to accurately detect the overall direction of motion). Each trial lasted for a maximum of 5 s, or until participants responded.

Measures of distance visual acuity, contrast sensitivity, and global motion detection were performed with an ML-PEST algorithm (Harvey 1997) implementing the maximum-likelihood adaptive staircase method for estimating sensory thresholds. The staircase fitted a new psychometric function to the data after each trial and ended after a 90% confidence level that the detection threshold estimate fell within ±0.1 log units of the true threshold measure. In all tasks, responses were given verbally by the participants and were encoded by the experimenter. Luminance readings and gamma correction were verified with a Minolta CS-100 Chroma Meter colorimeter on a regular basis.

Face/nonface categorization and face individuation. Face categorization and face individuation were assessed with three different sequential two-alternative forced choice delayed matching tasks (2AFC). Face categorization was assessed with full frontal faces (24 pictures, half male) and full front cars (24 pictures). Face individuation was assessed separately for full frontal faces (100 pictures) and depth-rotated (¾ profile) faces (96 pictures). In all three tasks, stimuli were grayscale and equalized for luminance with SHINEtoolbox (Willenbockel et al. 2010) implemented in MATLAB (MathWorks). Stimuli measured 300 pixels in height (~9.5° on the screen) with a width ranging between 200 and 265 pixels for faces (~7.5° on the screen) and between 350 and 400 pixels for cars (~12° on the screen). Pictures of faces were cropped for external features.

Each task consisted of the presentation of a stimulus in the center of the screen (360 ms in the categorization task, 500 ms in the individuation tasks) followed, after a 1,000-ms delay, by the central presentation of two stimuli arranged one on top of the other, which remained on the screen until a response was given. All tasks consisted of identifying, within each trial, which item had been presented at encoding. Participants were instructed to respond as accurately and as fast as possible. In the categorization task, 48 trials were administered in total. In half of the trials the encoding item was a face; in the other half the encoding item was a car. In the individuation tasks, the encoding face was always presented full-front whereas the subsequent faces were either full-front (in the front-front task) or depth-rotated (¾ profile, in the front-profile task). In both individuation tasks, the exact same faces were presented at upright and inverted (vertically flipped) orientations in four separate blocks (upright—inverted—inverted—upright) within each task. One hundred trials (half upright) were administered in the front-front task, and 96 trials (half upright) were administered in the front-profile task.

Both accuracy rates and correct response times (RTs) were considered for analyses. Accuracy rates (categorical values of 1 vs. 0 at each trial) were analyzed with binomial and χ^2-tests that were thus corrected for multiple comparisons. Correct RTs were first analyzed with ANOVAs and then with follow-up *t*-tests that were thus not corrected for multiple comparisons. One-tailed binomial tests were conducted on KL's accuracy scores within each session to test whether performance was significantly higher than chance. χ^2-Tests for independence were performed on accuracy scores to test for any significant between-session changes (individuation and categorization tasks) and to test for a face inversion effect within each session (individuation tasks). Only correct RTs that were below 2,000 ms (categorization task) or below 5,000 ms (individuation tasks) were considered for analyses and were ln-transformed to meet criterion of normal distribution for the use of parametric tests. ln-Transformed correct RTs that were below or above 3 standard deviations from the mean of each session were excluded. In the categorization task, KL's response speed across time was tested with a one-way repeated-measure ANOVA (and follow-up *t*-tests) with Session (Pre, Post 1.5m, Post 7m) as a within-subject factor. In the individuation tasks, a two-way between-groups ANOVA (and follow-up *t*-tests) were conducted on KL's ln-transformed correct RTs to explore the impact of Orientation (upright vs. inverted) and Session (Pre, Post 1.5m, Post 7m) on response speed.

In all the behavioral tasks, we used the modified *t*-test of Crawford et al. (2010) to compare KL's performance to the control subjects [i.e., visual acuity (Snellen decimal acuity), contrast sensitivity (%), global motion detection (%), and face categorization and face individuation (% and ms)]. This test is specifically designed to compare an individual's test score against norms derived from small control samples (Crawford et al. 2010). Here we used a *P* value of 0.05 within the framework of a unilateral hypothesis. Consequently, KL's thresholds, scores, and RTs associated with a one-tailed *P* value below 0.05 were considered as reflecting a significant difference relative to the control subjects. Analyses were conducted with a computerized version of the method (SINGLIMS_ES.exe).

fMRI Experiments

KL was scanned in three separate fMRI sessions lasting ~1.5 h each and consisting of four different experiments (1 functional run for each experiment) followed by the acquisition of a high-resolution anatomical image. Functional runs were block designs consisting of a motion localizer, a face localizer, and two auditory experiments. Before each fMRI acquisition, KL and the control subjects underwent a 45-min training session in a mock scanner. Recorded scanner noise was played in the bore of the simulator while KL and the control subjects practiced the tasks to familiarize themselves with the fMRI environment. In the scanner, visual stimuli were projected onto a mirror (127 mm × 102 mm) that was mounted at a distance of ~12 cm from the eyes of the participants. Auditory stimuli were delivered by means of circumaural, fMRI-compatible headphones (MR Confon, Magdeburg, Germany).

Motion localizer. The motion localizer run lasted 9 min and consisted of radially moving dots and static images of the same dots alternating in a block design with 18-s blocks that were each repeated

10 times. Stimuli in both conditions consisted of large white dots (~1.5° in the scanner) on a black background (~45° × 45° in the scanner), randomly placed at a minimum radius (~3° in the scanner) from a central white fixation cross (~2° × 2° in the scanner). Blocks were separated by a baseline (white fixation cross on a black background) lasting 7, 9, or 11 s (9 s on average). In the Motion blocks, six consecutive radially moving stimuli each lasting 3 s (1.5 s of expansion and 1.5 s of contraction) were presented [no interstimulus interval (ISI)] (dots' lifetime: 250 ms, velocity: ~15°/s in scanner). In the static blocks, six consecutive frames were presented in random order for 3 s each (no ISI). Occasionally, the background color of the display changed from black to gray for 500 ms. The task consisted of detecting that color change and pressing a response key with the right index finger. Within each condition, there were three blocks with one target, three blocks with two targets, and three blocks with no targets.

Face localizer. The face localizer run lasted 15 min and consisted of eight repetitions of each of the four conditions, alternating in blocks of 19.35 s. Blocks were separated by a baseline condition (white fixation cross of ~2° × 2° on a black background) lasting 7, 9, or 11 s (9 s on average). Each condition consisted of a different category: faces, cars, and their phase-scrambled version (identical amplitude in each frequency band; Sadr and Sinha 2004). Stimuli were identical to those used in Rossion et al. (2012). In each block, 43 images (210 × 184 pixels, ~20° width × 25° height in the scanner) were presented on a black background for 380 ms with a 70-ms ISI. Occasionally, a picture was replaced by a uniform gray rectangle (380 ms) that the participant had to detect by pressing a key with the right index finger. Within each condition, there were three blocks with one such target, two blocks with two such targets, and three blocks with no targets.

Auditory experiment 1: voices vs. horizontally moving sounds. Participants were instructed to keep their eyes closed during this run. The run lasted ~13 min and consisted of 15 repetitions of each of the two conditions alternating in blocks of 16.8 s. Blocks were separated by rest periods of 7, 9, or 11 s (9 s on average). The two conditions consisted of voices and moving sounds that were matched for low-level properties. Human voices were 700-ms (695 ms + 5 ms silence) vowels ("a," "e," "i," "o," "u") pronounced by 12 different francophone speakers (half male) and normalized for overall RMS. Vowels were concatenated (no ISI) into 15 blocks. Each block of horizontally moving sounds consisted of a frequency-scrambled version of a vocal block that was created by randomly intermixing the amplitude and frequency of each Fourier component (Belin et al. 2000) within frequency windows of 150 Hz. Envelopes consisting of linear ramps going from 0 to maximal intensity and from maximal intensity to 0 every 700 ms were then applied on each scrambled block separately for the left and the right ear. This resulted in a stereo sound where intensity increased in one ear and decreased simultaneously in the other ear, creating the vivid perception of a sound moving from one ear to the other in the azimuth every 700 ms. The task was to detect a target stimulus (either a vowel or a moving sound) that lasted longer (1,400 ms) and press a response key with the right index finger. Within each condition, there were five blocks with one target (23 stimuli total), five blocks with two targets (22 stimuli total), and five blocks with three targets (21 stimuli total).

Auditory experiment 2: spatial vs. pitch discrimination. Stimuli and paradigm were identical to the those used in previous studies of our group (see Collignon et al. 2011b, 2013 for a full description of the procedure). Participants that were tested in these studies were blindfolded at that time. However, because KL in the present study had to perform visual experiments within the same scanning session, she was simply instructed to keep her eyes closed during this run. During both auditory runs, the scanning room was put in complete darkness by shutting down the light of the room and of the projector, resulting in complete obscurity and ensuring that no light was perceived through the closed eyelids.

MRI/fMRI Data Acquisition

The fMRI series were acquired with a 3-T TRIO TIM system (Siemens) equipped with a 12-channel head coil. Multislice T2*-weighted fMRI images were obtained with a gradient echo-planar sequence using axial slice orientation [time to repetition (TR) 2,200 ms; echo time (ET) 30 ms; flip angle (FA) 90°; 35 transverse slices; 3.2-mm slice thickness; 0.8-mm (25%) interslice gap; field of view (FoV) 192 × 192 mm^2; matrix size 64 × 64 × 35; voxel size 3 × 3 × 3.2 mm^3]. The three (in all runs except *auditory experiment 2*) or four (in *auditory experiment 2*) initial scans were discarded to allow for steady-state magnetization. A structural T1-weighted 3D magnetization prepared rapid gradient echo sequence (voxel size 1 × 1 × 1.2 mm^3; matrix size 240 × 256; TR 2,300 ms; ET 2.91 ms; TI 900 ms; FoV 256; 160 slices) was also acquired in each session. Online prospective head motion correction methods were not available for the structural MRI (Maclaren et al. 2013). Image quality of the structural data was assessed qualitatively by the technical radiologist after each acquisition to decide whether any visible artifacts (including head motion, RF interference, wraparound, and signal intensity of contrast inhomogeneities) made repetition necessary. Image quality was also quantitatively assessed with a retrospective entropy-based autofocusing method developed by Aksoy and colleagues (2012) for rigid head motion correction (see also Schulz et al. 2012). This analysis revealed that the quality of the structural images obtained from KL were of equal or, if anything, better quality than in the control subjects who were scanned twice. Moreover, the difference in quality [delta average edge strength (ΔAES)] between sessions was minor and, if anything, lower than the differences obtained in the control subjects.

Functional volumes were preprocessed and analyzed with SPM8 (Welcome Trust Centre for Neuroimaging, London, UK; http://www.fil.ion.ucl.ac.uk/spm/) implemented in MATLAB (MathWorks). Preprocessing included the realignment of functional time series, the coregistration of functional and anatomical data, a spatial normalization to an echo planar imaging template conforming to Montreal Neurological Institute (MNI) space, and a spatial smoothing [8-mm full width at half-maximum (FWHM) isotropic Gaussian kernel].

MRI Data Analysis: Voxel-Based Morphometry

Anatomical images acquired in the Pre, Post 1.5m, and Post 7m sessions were preprocessed with the vbm8 toolbox of SPM8 (Welcome Trust Centre for Neuroimaging; http://www.fil.ion.ucl.ac.uk/spm/). The "Process Longitudinal Data" module, taking into account the characteristics of intrasubject analysis, was used to perform these analyses. After an initial realignment of the anatomical images from the three sessions, the mean image was calculated and was used as a reference image for a subsequent realignment. Realigned anatomical images were then corrected for signal inhomogeneity with regard to the reference (mean) image. Bias-corrected realigned images from each session were segmented into gray matter, white matter, and cerebrospinal fluid. This procedure resulted in a set of nine images (3 tissue probability maps for each of the 3 sessions) in the same space as the original T1-weighted image, in which each voxel was assigned a probability of being gray matter, white matter, and cerebrospinal fluid, respectively. These images were spatially smoothed with an 8-mm (FWHM) isotropic Gaussian kernel.

To estimate the variability of the measure that should be expected (noise error) when comparing gray matter tissue probability maps from anatomical images acquired on separate sessions, we performed identical analyses on the anatomical images of nine normally sighted participants who were scanned on two separate occasions (*scan 1* and *scan 2*).

Statistical analyses were computed as follows. First, we calculated between-session differential images in KL and in each control subject with the ImCalc function implemented in SPM8. This led to three differential images in KL (Post 7m − Pre, Post 1.5m − Pre, Post 7m

− Post 1.5m) (see Fig. 2, *A* and *B*) and one differential image in each control subject (*scan 2* − *scan 1*). Second, for each of these 13 differential images, we calculated the mean and standard deviation of the distribution of differential values obtained within each voxel across the brain (see Fig. 2, *A* and *B*). As expected, means of absolute differences (increases or decreases) between *scan 1* and *scan 2* in control subjects were close to 0, with a change of 0.4% on average (range = min. 0.15%–max. 0.82%, SD = 0.25%). Similarly in KL, mean absolute between-session differences were 0.08% (within normal range) in the Post 7m − Post 1.5m differential image. In contrast, mean absolute between-session differences in KL in Post 1.5m and Post 7m relative to Pre were 1.32% and 1.22%, respectively, >3 SD above the mean of controls. Thus only the latter differential images were considered for further analyses in KL. Across KL's brain, we defined voxels showing significant differences at Post 1.5m relative to Pre and at Post 7m relative to Pre as those displaying the largest 1% increases or decreases within each differential image (±3 SD from the mean of the distribution of changes; see gray shaded areas in Fig. 2, *A* and *B*). Finally, to ensure the reliability of the changes across sessions, we reported only those voxels that passed the statistical threshold in both Post 1.5m and Post 7m sessions relative to Pre [i.e., voxels showing significant gains/losses both in Post 1.5m (≥8.07%/≤−5.43%) and Post 7m (≥8.45%/≤−6.01%) relative to Pre] (see Fig. 2*C*).

fMRI Data Analysis

Analyses of fMRI data in KL (3 sessions) and in control subjects (1 session, see *General Experimental Design and Control Participants*) were performed based on a mixed-effects model and were conducted in a single step accounting for fixed effects. Changes in brain regional responses in KL were estimated by a general linear model including 6 regressors in the motion localizer (2 conditions × 3 sessions), 12 regressors in the face localizer (4 conditions × 3 sessions), and 6 regressors in each of the two auditory experiments (2 conditions × 3 sessions). In the control subjects, changes in brain regional responses were estimated by a general linear model including two regressors in the motion localizer, four regressors in the face localizer, and two regressors in each of the two auditory experiments. These regressors consisted of a boxcar function convolved with the canonical hemodynamic response function. For each session, the movement parameters derived from realignment of the functional volumes (translations in the *x*, *y*, and *z* directions and rotations around the *x*-, *y*-, and *z*-axes) and a constant vector were included as covariates of no interest. In addition, for each session of *auditory experiment 2*, the instructions preceding each block were further included as a covariate of no interest. High-pass filtering was implemented in sessions with a cutoff period of 128 s to remove slow drifts from the time series. Serial correlations in fMRI signal were estimated with an autoregressive (order 1) plus white noise model and a restricted maximum likelihood (ReML) algorithm.

In control subjects (1 session), contrasts of interest in each of the four experimental runs were performed as follows. In the motion localizer, the contrast [Motion > Static] identified motion-specific responses. In the face localizer, a conjunction analysis was performed in order to identify face-specific responses relative both to scrambled faces and to cars [Faces > ScrFaces ∩ Faces > Cars] (Rossion et al. 2012). In *auditory experiment 1*, the contrast [Motion + Voice] tested the global processing of sounds and the contrasts [Motion > Voice] and [Voice > Motion] tested specific processing of motion and voices. Finally, in *auditory experiment 2*, the contrast [Spatial + Pitch] tested the global processing of sounds and the contrasts [Spatial > Pitch] and [Pitch > Spatial] tested specific processing of spatial and pitch attributes of sounds (Collignon et al. 2011b, 2013).

In KL (3 sessions), analyses were performed in two steps. First, a conjunction (AND) analysis between sessions [Pre ∩ Post 1.5m ∩ Post 7m] was performed on contrasts of interest (as described in the preceding paragraph) to identify regions that were consistently activated in a given contrast across sessions. In the face localizer, the conjunction was performed across sessions [Pre + Post 1.5m + Post 7m] to identify face-specific responses relative both to scrambled faces and to cars when considering all sessions [Faces all sessions > ScrFaces all sessions ∩ Faces all sessions > Cars all sessions] (Rossion et al. 2012). Second, between-session comparisons on contrasts of interest were performed with linear contrasts.

Statistical inferences on the *t*-statistics maps resulting from contrasts of interest were performed at a threshold of $P < 0.05$ after correction for multiple comparisons over the whole brain (familywise error method) or over small spherical volumes (15-mm radius) located in regions of interest [small volume correction (SVC)]. Significant clusters extended to at least 10 contiguous voxels—unless localized in regions of interest—and were anatomically labeled using structural neuroanatomy information provided by the Anatomical Automated Labeling (AAL) toolbox (Tzourio-Mazoyer et al. 2002) and Pickatlas (Maldjian et al. 2003). Automatic labeling was systematically and carefully checked. To ensure reliability of the changes across sessions in KL, between-session comparisons of brain responses in Pre vs. Post 1.5m sessions and in Post 1.5m vs. Post 7m sessions were masked inclusively ($P_{uncorr} < 0.001$) by the between-session contrast comparing brain responses in Pre vs. Post 7m sessions. Hence, we only included regions showing between-session changes that were consistent over time (e.g., regions showing a differential effect when comparing Pre vs. Post 1.5m for a given contrast but no differential effect when comparing Pre vs. Post 7m for the same contrast would not be included).

To illustrate brain responses to sounds within KL's primary visual cortex, 13 spheres of 6-mm radius were traced along the calcarine sulcus including its lower and upper banks, in steps of 3 mm along the *y*-axis, from the most caudal part ($y = -96$) to the most rostral part ($y = -60$). Using the MarsBar toolbox (Brett et al. 2002), *t*-values were extracted in each of these regions of interest (see for similar analyses Dormal et al. 2010; Mahon et al. 2009; Tootell et al. 2008). Finally, to illustrate the strength of auditory-driven activity in primary visual cortex in KL relative to early blind, late blind, and sighted control participants, we extracted estimated auditory activity in *auditory experiments 1* and *2* within an anatomical mask encompassing the primary visual cortex around the calcarine fissure (delivered by MarsBar toolbox; Brett et al. 2002).

SVC (15-mm sphere) was only used in the face localizer to identify face-selective regions. SVCs were performed on coordinates reported in Rossion et al. (2012), who used stimuli and analyses identical to the present study. As coordinates in that paper were reported in Talairach space, we first transformed them in MNI space, using Matthew Brett's bilinear transformation (http://imaging.mrc-cbu.cam.ac.uk/imaging/MNITalairach), before performing the SVCs. Standard stereotactic coordinates were as follows: right fusiform gyrus (37, −48, −15) and right inferior occipital gyrus (38, −72, −11).

RESULTS

Behavioral Results

Far visual acuity. At Pre, KL's best-corrected distance visual acuity expressed in Snellen decimal acuity was 0.04 in the right (operated) eye (Fig. 1*A*). The success of the surgery was witnessed as improvements in visual acuity as early as 1.5 mo after surgery. Acuity in the right eye increased to 0.2 at Post 1.5m and to 0.7 at Post 7m. At all times, distance visual acuity in the left eye was too low to be tested. In fact, distance visual acuity for binocular vision (OU) was identical to that measured in the right (operated) eye (OD). Even at Post 7m, KL's acuity remained significantly below normal range (OU: $t = -3.3$, OD: $t = -2.9$, both $P < 0.05$).

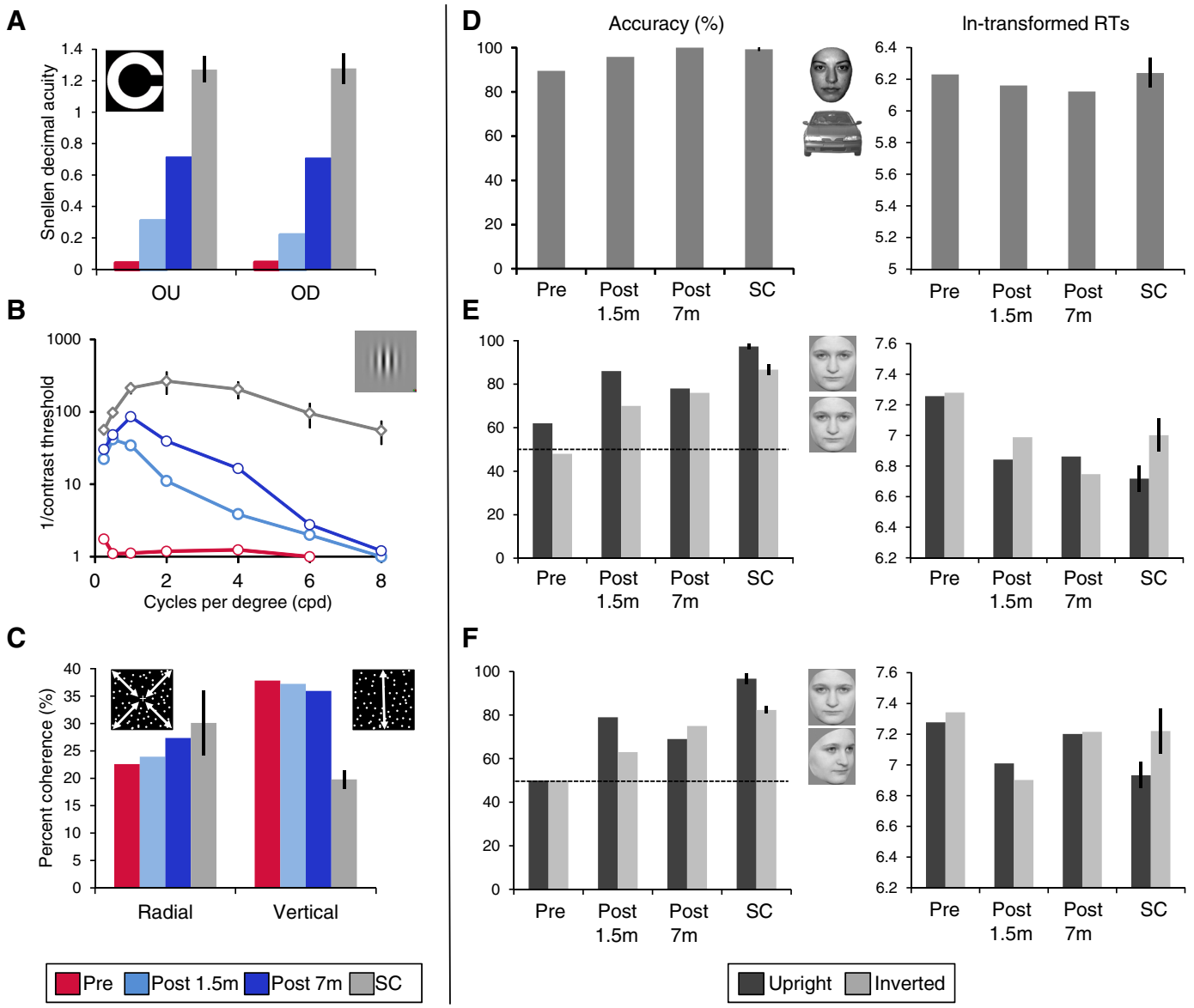

Fig. 1. Behavioral performance in KL (at Pre, Post 1.5m, and Post 7m) and in sighted control subjects (SC). *A*: distance visual acuity measures expressed in Snellen decimal acuity obtained in the Landolt-C paradigm for binocular (OU) and right (operated) eye (OD). *B*: contrast sensitivity function (CSF). *C*: % coherence thresholds for radial and vertical global motion detection. *D–F*: % accuracy and ln-transformed correct response times (RTs) in the face categorization task (*D*) and the front-to-front (*E*) and front-to-profile (*F*) face individuation tasks, separately for upright and inverted faces. Bars represent SE from the mean.

Contrast sensitivity function. KL's CSF before surgery was essentially flat, with a resolution limit of 6 cpd (Fig. 1*B*). A substantial and selective improvement for low spatial frequencies was observed at Post 1.5m and Post 7m. Between 1.5 and 7 mo after surgery, contrast sensitivity did not improve further for spatial frequencies up to 0.5 cpd, but there were improvements for spatial frequencies from 1 to 4 cpd at Post 7m relative to Post 1.5m. KL's contrast sensitivity at all spatial frequency ranges was well below normal range in all sessions (all $P < 0.00001$) except for 0.25 cpd at Post 7m (0.25 cpd, $t = 2.798$, $P = 0.053$).

Global motion. KL's coherence thresholds were stable across the three sessions in both the radial and the vertical conditions (Fig. 1*C*). In the radial condition thresholds measured in each session (Pre = 22.6%, Post 1.5m = 23.9%, Post 7m = 27.4%) were comparable to normal control subjects' thresholds (30%, all $P > 0.3$), whereas in the vertical condition, thresholds were higher (worse performance) for KL (Pre = 37.8%, Post 1.5m = 37.2%, Post 7m = 35.9%) compared with control subjects (19.8%, all $P < 0.02$).

Face categorization and individuation. KL performed well in the face vs. car categorization task in all sessions (Fig. 1*D*), with accuracy being significantly below the control subjects only at Pre ($t = -7.432$, $P = 0.009$; other P values > 0.06). KL was as fast as the control subjects in all sessions (all $P > 0.3$). The effect of Session did not reach significance either in accuracy rates [χ^2 (2, $n = 140$) = 5.706, $P = 0.06$] or in correct RTs [$F(2,80) = 2.913$, $P = 0.06$].

In the front-to-front (FF) and the front-to-profile (FP) individual face discrimination tasks, KL performed at chance prior to surgery in both orientations and in both tasks (all $P > 0.06$). After surgery, she performed significantly above chance level

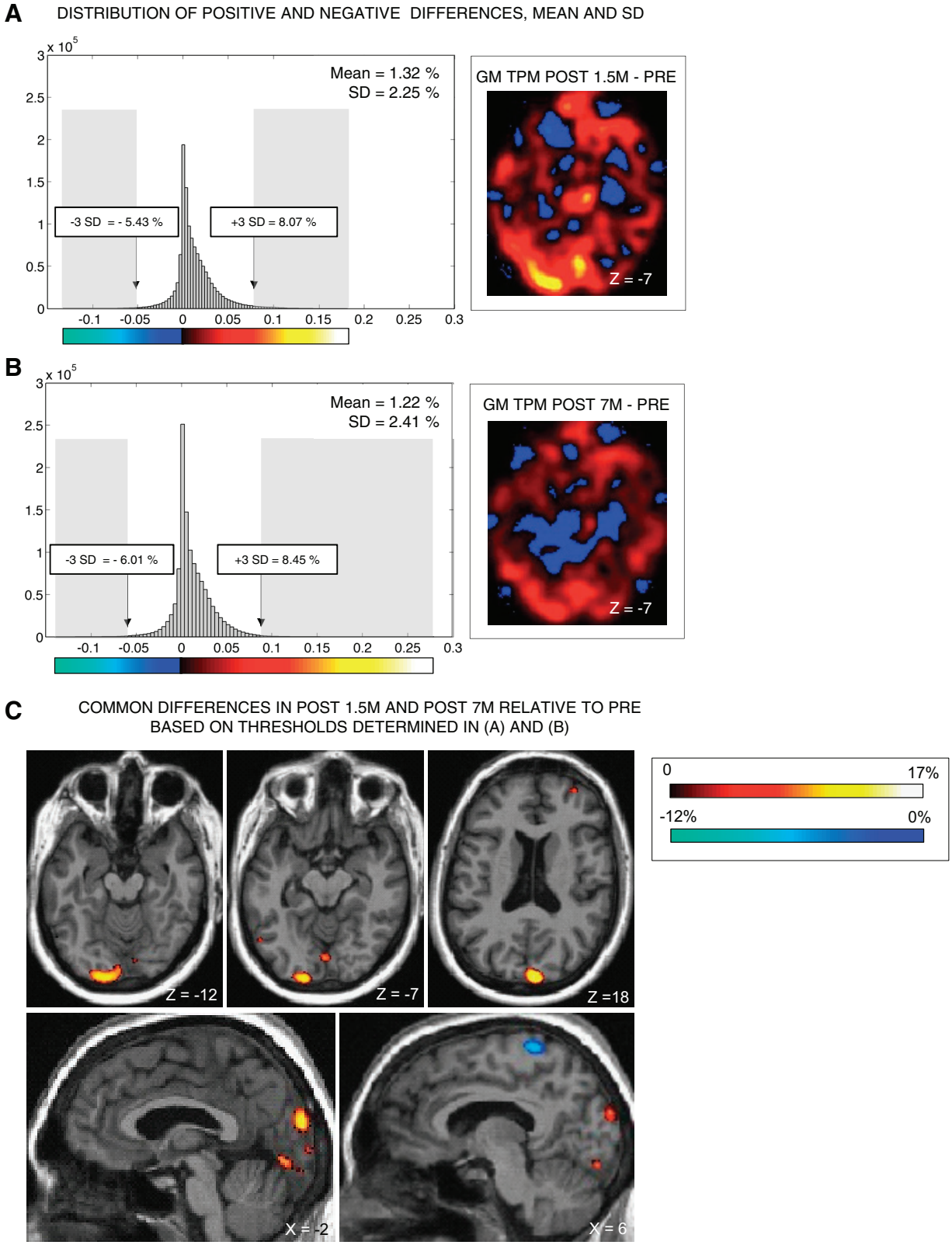

Fig. 2. Voxel-based morphometry (VBM) analyses and results. *A* and *B*: VBM analyses in KL. The smoothed gray matter tissue probability map (GM TPM) obtained at Pre was subtracted from the smoothed GM TPM obtained at Post 1.5m (*A*) and at Post 7m (*B*). Thresholds for significant differences were established based on the mean and SDs of the distribution of positive and negative differences observed in the differential image obtained in *A* and *B*. *C*: only voxels showing common between-session differences above or below 3 SDs from the mean of the distribution in *A* and *B* are reported, by overlapping the thresholded differential image on KL's native anatomical image.

(all $P < 0.007$) except in the FP task at Post 1.5m, where performance with inverted faces was not significantly higher than chance ($P = 0.055$) (Fig. 1, *E* and *F*). Identical conclusions resulted after application of Bonferroni correction for multiple comparisons.

Because KL performed at chance before surgery in both tasks and with both orientations, we conducted subsequent analyses only on postsurgery data. There was no significant change in accuracy between Post 1.5m and Post 7m either for upright faces [FF: χ^2 (1, $n = 100$) = 0.61, $P = 0.44$; FP: χ^2 (1, $n = 96$) = 0.865, $P = 0.35$] or for inverted faces [FF: χ^2 (1, $n = 100$) = 0.203, $P = 0.65$; FP: χ^2 (1, $n = 96$) = 1.212, $P = 0.27$]. In the FF task, KL was faster overall at Post 7m compared with Post 1.5m [$F(1,150) = 6.89$, $P = 0.01$] but slower at Post 7m relative to Post 1.5m in the FP task [$F(1,132) = 20.77$, $P < 0.001$]. Accuracy with upright faces remained significantly below normal range in both tasks after surgery (all $P < 0.035$), whereas performance with inverted faces was below normal range at Post 1.5m (FF: $t = -3.468$, $P = 0.037$; FP: $t = -5.489$, $P = 0.015$) but not at Post 7m (FF: $t = -2.22$, $P = 0.07$; FP: $t = -2.081$, $P = 0.086$). KL was as fast as the control subjects in both tasks at Post 1.5m and Post 7m (all $P > 0.13$).

Some control subjects showed an inversion effect—a lower performance for inverted than upright faces (Rossion 2008)—in accuracy [FF: *Ctrl2* χ^2 (1, $n = 100$) = 4.43, $P = 0.035$; FP: *Ctrl1* χ^2 (1, $n = 96$) = 4.41, $P = 0.036$; *Ctrl2* χ^2 (1, $n = 96$) = 5.55, $P = 0.019$], and all showed an inversion effect in correct RTs in both tasks (all $P < 0.001$). Importantly, KL did not show any significant inversion effect after surgery in accuracy in any task (all $P > 0.09$). In the FP task, she showed no inversion effect in correct RTs (main effect of Orientation and interaction not significant, $P > 0.25$). In the FF task, the interaction between Session and Orientation was significant [$F(1,150) = 9.613$, $P = 0.002$] because of faster RTs for upright faces than for inverted faces at Post 1.5m [$t(76) = 2.27$, $P = 0.026$] and faster RTs for inverted faces than for upright faces at Post 7m [$t(74) = -2.13$, $P = 0.036$].

In summary, individual face discrimination was at chance prior to surgery and was significantly above chance level for both upright and inverted faces 7 mo after surgery. However, performance remained quantitatively below (for upright faces at least) and qualitatively different from normal control subjects, as there was no consistent evidence of a face inversion effect in KL.

Voxel-Based Morphometry Results

Because of the well-known impact of perceptual experience on brain structure (Zatorre et al. 2012), we investigated potential morphological changes associated with sight restoration with voxel-based morphometry. Gray matter density increases were consistently observed at Post 1.5m and Post 7m relative to Pre in several occipital regions including bilateral pericalcarine cortex and lingual gyri, left middle occipital gyrus, and right cuneus (Fig. 2*C*, Table 1).

fMRI Results

Visual motion localizer. Target detection performance (hits vs. misses) was high in all sessions, with no difference between sessions [Pre, Post 1.5m, Post 7m: 100%, 94%, 94%, χ^2 (2, $n = 54$) = 1.038, $P = 0.59$].

A conjunction (AND) analysis identified a large set of regions that consistently responded to radially moving relative

Table 1. *VBM results*

Area	Native Space			Change, %	Cluster Size	MNI Space		
	x, mm	*y*, mm	*z*, mm			*x*, mm	*y*, mm	*z*, mm
Gray matter density increases in Post 1.5m and Post 7m relative to Pre								
R cerebellum	27	−55	−35	17.47	3,823	35	−62	−43
L pericalcarine cortex/middle occipital gyrus	−16	−89	−8	12.17	1,296	−16	−99	0
L cerebellum	−27	−59	−32	13.07	1,049	−30	−68	−37
R cuneus	1	−83	17	15.15	590	6	−88	29
R mid frontal gyrus	26	39	7	9.82	235	29	56	−14
L fusiform gyrus	−16	3	−29	11.07	169	−20	6	−45
R putamen	23	−13	13	11.22	153	28	−7	9
L pericalcarine/lingual gyrus	−1	−73	−5	9.79	112	1	−79	−1
R inf temporal gyrus	40	−20	−21	9.88	59	51	−18	−31
R mid frontal gyrus	26	36	14	9.13	55	29	54	−4
L inferior occipital/temporal gyrus	−46	−62	−8	8.86	34	−53	−69	−4
L sup frontal gyrus	−8	31	−3	9.04	29	−13	43	−24
L mid frontal gyrus	−32	−6	51	9.17	22	−41	8	56
R lingual gyrus	6	−76	−10	8.95	18	10	−83	−8
L pericalcarine cortex	−3	−87	0	8.90	14	−1	−95	9
Gray matter density decreases in Post 1.5m and Post 7m relative to Pre								
L cerebellum	−17	−46	−40	−12.92	1,057	−18	−54	−50
R postcentral gyrus	7	−41	56	−7.73	354	13	−32	68
L cerebellum	−40	−44	−33	−7.75	153	−46	−52	−41
R postcentral gyrus	23	−32	50	−7.19	74	34	−25	58
L paracentral lobule	−16	−41	53	−6.65	29	−16	−32	66
L dorsolateral superior frontal gyrus	−6	38	23	−5.73	7	−11	58	7

Summary of the between-session gray matter changes obtained in the voxel-based morphometry (VBM) results. Significant clusters are reported in KL's native space coordinates and in Montreal Neurological Institute (MNI) space coordinates.

to static dots across the three sessions ([Motion > Static Pre ∩ Post 1.5m ∩ Post 7m]) (Fig. 3*A*, Table 2). In line with previous studies investigating visual-motion selectivity (Sunaert et al. 1999; Tootell et al. 1995), these regions included the middle temporal cortex (MT+/V5), the superior occipital gyrus (V3/V3A), and the superior temporal gyrus bilaterally as well as the left middle occipital gyrus (LOS/KO). Similar activation maps were observed in our control participants scanned with the same protocol (see Fig. 7*A*). In KL, between-session increases in motion-selective activity were observed at Post 7m relative to Pre ([Motion > Static × Post 7m > Pre]) in bilateral extrastriate cortices along the motion pathway localized posteriorly to MT+/V5: the middle occipital gyri bilaterally extending medially to the superior occipital gyri/cuneus (V2/V3/V3A) [Motion > Static Post 7m > Pre] (Fig. 3*B*, Table 2). No such changes were observed in bilateral MT+/V5 (Fig. 3*B*).

Face localizer. Target detection performance (hits vs. misses) was high in all sessions, with no difference between sessions [Pre, Post 1.5m, Post 7m: 89%, 89%, 71%, $\chi\chi^2$ (2, $n = 84$) = 5.227, $P = 0.073$].

Before surgery, regions in fusiform and inferior occipital gyri showed a preference for faces over cars and scrambled faces ([Faces Pre > ScrFaces Pre ∩ Faces Pre > Cars Pre]) (see Fig. 7*B*) with no significant changes across time (Table 3). Hence, a conjunction (AND) analysis was performed across sessions [Faces all sessions > ScrFaces all sessions ∩ Faces all sessions > Cars all sessions] (Rossion et al. 2012) and disclosed face selectivity in bilateral inferior occipital gyrus ("occipital face area" or OFA) and in the right fusiform gyrus ("fusiform face area" or FFA) (Fig. 4, Table 3), in accordance with previous neuroimaging studies of face perception (Haxby et al. 2000) and with activation maps observed in our sighted control participants scanned with the same protocol (see Fig. 7*B*).

Auditory experiments. Behavioral performance in the scanner was adequate in both auditory experiments in all sessions (*auditory experiment 1*: 73%, 70%, 88%; *auditory experiment 2*: 63%, 63%, 74%). Performance was significantly higher at Post 7m compared with Post 1.5m in *auditory experiment 1* [χ^2 (2, $n = 180$) = 6.088, $P = 0.048$; Post 1.5m vs. Post 7m: χ^2 (1, $n = 120$) = 6.114, $P = 0.013$] and compared with both Pre

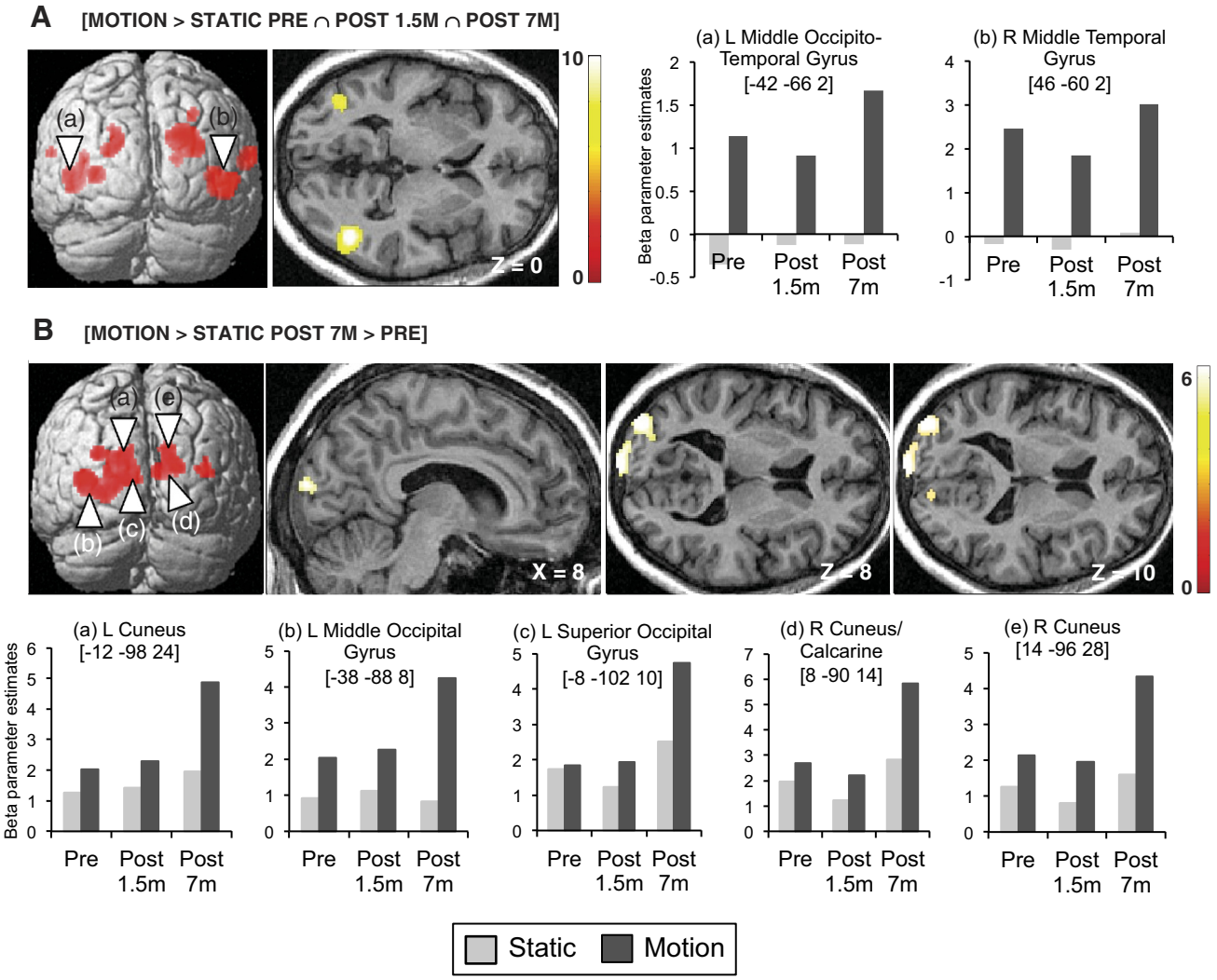

Fig. 3. fMRI activation maps of visual motion processing. *A*: between-session conjunction analysis highlighting regions showing consistent motion-specific responses [Motion > Static] across the 3 sessions in KL and associated beta parameter estimates in bilateral MT+/V5. *B*: brain regions showing larger motion-specific visual responses [Motion > Static] at Post 7m relative to Pre and associated beta parameter estimates. Results are displayed at a threshold of $P < 0.05$ familywise error (FWE) corrected over the whole brain on a 3D render of the brain and on transverse and sagittal slices of KL's structural image normalized to MNI space.

Table 2. *Motion localizer fMRI results*

Area	Cluster Size	*x*, mm	*y*, mm	*z*, mm	*Z*	*P*
Conjunction [Motion > Static Pre ∩ Post 1.5m ∩ Post 7m]						
R middle temporal gyrus (MT+/V5)	404	46	−60	2	Inf	<0.001
R superior temporal gyrus	129	62	−28	14	7.74	<0.001
L middle occipito-temporal gyrus (MT+/V5)	225	−42	−66	2	7.46	<0.001
R middle/superior occipital gyrus	314	34	−90	24	7.08	<0.001
L middle occipital gyrus	79	−30	−86	6	6.72	<0.001
L superior occipital gyrus	121	−16	−86	26	6.26	<0.001
L superior temporal gyrus	18	−58	−42	18	5.62	0.001
R superior occipital gyrus	21	30	−78	44	5.30	0.003
[Motion > Static Post 1.5m > Pre]						
No suprathreshold voxels						
[Motion > Static Post 7m > Pre]						
L middle occipital gyrus	737	−38	−88	8	6.22	<0.001
L cuneus		−12	−98	24	6.04	<0.001
L superior occipital gyrus		−8	−102	10	6.04	<0.001
R cuneus	239	14	−96	28	5.84	<0.001
R cuneus/calcarine		8	−90	14	5.60	0.001
R superior occipital gyrus		20	−100	18	5.51	0.001
R middle occipital gyrus	39	38	−88	14	5.27	0.004
[Motion > Static Post 7m > Post 1.5m]						
L middle occipital gyrus	596	−40	−86	10	6.71	<0.001
R cuneus	135	8	−86	20	6.61	<0.001
L cuneus/superior occipital gyrus	149	−10	−94	22	6.43	<0.001
R middle occipital gyrus	177	36	−78	18	5.81	<0.001
L inferior occipital/fusiform gyrus	32	−42	−70	−14	5.81	<0.001
R inferior occipital gyrus	21	52	−70	−2	5.53	0.001
R inferior occipital gyrus	12	38	−82	−4	5.01	0.013

Table 2. Summary of the functional results obtained for the specific responses to visual motion relative to static dots (Motion > Static). All coordinates reported in this table are significant after correction over the entire brain [familywise error (FWE) $P < 0.05$].

and Post 1.5m in *auditory experiment 2* [$F(2,28) = 6.083$, $P = 0.006$; Pre vs. Post 7m: $t(14) = -2.876$, $P = 0.012$; Pre vs. Post 1.5m $t(14) = -2.825$, $P = 0.014$].

In both auditory experiments, several occipital regions were consistently recruited during the processing of auditory information across the three sessions in KL ([Motion + Voice Pre ∩ Post 1.5m ∩ Post 7m]; [Spatial + Pitch Pre ∩ Post 1.5m ∩ Post 7m]) (Fig. 5, *A* and *B*, Table 4, Table 5). These regions were localized along the calcarine sulcus extending medially to the cuneus and to the lingual gyrus (Fig. 5, *A* and *B*, Table 4, Table 5). In both auditory experiments, peaks of activation to global auditory processing in KL's primary visual cortex were located in the caudal part of the calcarine sulcus and *t* values steadily decreased along the calcarine sulcus when sliding to its most rostral part (Fig. 5, *A* and *B*). Importantly, significant auditory responses in pericalcarine regions were also observed in early and late blind participants (tested with the same protocol as in *auditory experiment 2*; Collignon et al. 2011b, 2013) but not in normally sighted participants (tested with the same protocols as in *auditory experiments 1* and *2*) (Fig. 5*C*; see Fig. 7, *C* and *D*).

Despite the fact that auditory activity was still massively present 7 mo after surgery in striate cortex (Fig. 5, *A–C*), the recruitment of occipital cortex for auditory processing steadily decreased relative to before surgery ([Motion + Voice × Pre > Post 7m]; [Spatial + Pitch × Pre > Post 7m]), especially in extrastriate regions, including the bilateral middle occipital gyri in both auditory experiments as well as the bilateral superior occipital gyri and lingual gyri in *auditory experiment 2* (Fig. 5, *D* and *E*, Table 4, Table 5). Beta parameter estimates in these regions highlight a progressive reduction of activation in response to auditory stimulation with time, with some of these regions even showing sound-related deactivation at Post 7m (Fig. 5, *D* and *E*).

No consistent functional specialization (selective auditory activity for a specific task) was found in KL's occipital cortex in either of the two auditory experiments across sessions (i.e., contrast between Motion and Voice conditions in *auditory experiment 1* and between Spatial and Pitch conditions in *auditory experiment 2*; Collignon et al. 2011b, 2013).

DISCUSSION

In the present study, we provide a comprehensive overview of the changes occurring in perceptual visual abilities as well as in brain structure and function in an early and severely visually impaired patient, KL, before and after sight restoration. KL was tested in three separate sessions taking place before and 1.5 and 7 mo after surgery with identical behavioral, MRI, and fMRI protocols. The extent of KL's preoperative visual impairments was evidenced by extremely reduced visual acuity (0.04) and CSF before surgery (Fig. 1, *A* and *B*). Nevertheless, presurgical global motion detection (radial patterns) and face/nonface categorization abilities were accurate (Fig. 1, *C* and *D*) and sufficient to elicit specific functional responses within high-level visual areas involved in motion and face processing (Fig. 3*A*, Fig. 4; see Fig. 7, *A* and *B*). Despite these residual visual functions, robust crossmodal auditory responses were observed within KL's occipital cortex before surgery. These crossmodal responses were at least as high as those measured in totally blind individuals (Fig. 5*C*; see Fig. 7*D*). In pericalcarine cortex, crossmodal responses remained elevated even 7 mo after surgery (Fig. 5, *A–C*) and overlapped with visual responses (Fig. 6).

The success of the surgery was evidenced by behavioral improvements in visual acuity, sensitivity to low-spatial fre-

Table 3. *Face localizer fMRI results*

Area	Cluster Size	*x*, mm	*y*, mm	*z*, mm	*Z*	*P*
Conjunction [Faces > ScrF ∩ Faces > Cars all sessions]						
L inferior occipital gyrus (OFA)	101	−50	−76	−6	6.50	<0.001
R inferior occipital gyrus (OFA)*	20	42	−72	−4	3.93	0.011
R fusiform gyrus (FFA)*	7	34	−52	−20	3.31	0.074

Summary of the functional results obtained for the specific responses to Faces relative to both Scrambled Faces (ScrF) and Cars. There were no significant activations in any of the between-session comparisons. Coordinates are significant after correction over the entire brain (FWE $P < 0.05$) or over small spherical volumes (15-mm radius). OFA, occipital face area; FFA, fusiform face area.

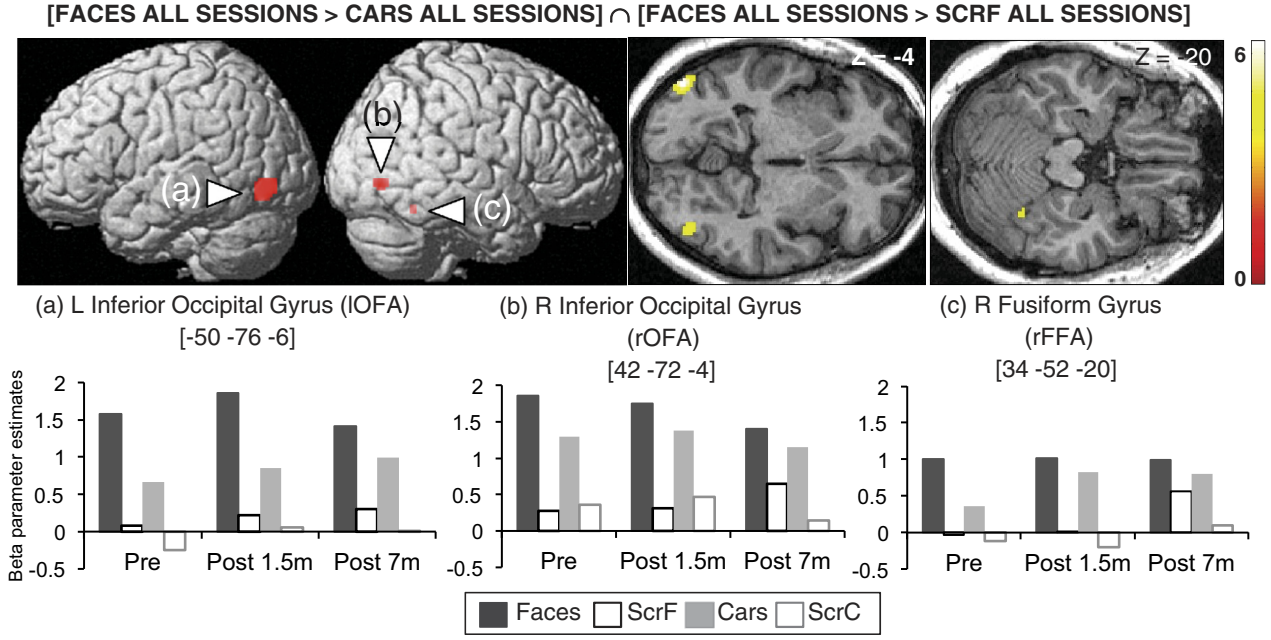

Fig. 4. fMRI activation maps of face processing: brain regions responding more to Faces relative to both Cars and Scrambled Faces (ScrF) in all sessions in KL and associated beta parameter estimates. Results are displayed at a threshold of $P < 0.001$ uncorrected on a 3D render of the brain and on transverse slices of KL's structural image normalized to the Montreal Neurological Institute (MNI) space. ScrC, Scrambled Cars; OFA, occipital face area; FFA, fusiform face area.

quencies, and face individuation (Fig. 1, *A*, *B*, *E*, and *F*), as well as by significant increases in neural responses to radially moving patterns in low-level visual regions (Fig. 3*B*). Whether these gains were purely optical in origin or were the result of neural plasticity cannot be fully disentangled in such a study because of the intrinsic covariation existing between these factors. However, robust neuroplastic changes were evidenced as a result of sight restoration: crossmodal auditory responses progressively decreased in extrastriate occipital regions after surgery relative to before surgery (Fig. 5, *D* and *E*), and significant increases in gray matter density were observed in low-level visual cortex as early as 1.5 mo after surgery (Fig. 2*C*).

Presurgical Visual Selective Responses in High-Level Visual Cortex Involved in Motion and Face Processing

In accordance with the observation of normal presurgical performance in global motion detection thresholds for radially moving patterns and in face/nonface categorization, motion- and face-selective responses were found within well-documented regions of the dorsal and the ventral visual pathway in KL before surgery and did not significantly evolve after surgery. These findings suggest that functionally specific responses have emerged in KL's high-level visual cortex during development despite a life-long history of severely degraded visual experience.

In the case of motion-selective responses, this assumption is supported by the fact that MT+ receives most of its input from the magnocellular pathway (Maunsell et al. 1990) and may thus have tuned during development based on KL's residual sensitivity to low spatial frequencies. Since our behavioral results suggest a dissociation in the way visual impairment impacts specific types of motion (i.e., preservation in perception of radial motion but impairment in perception of vertical motion), future studies should investigate whether perceptual dissociations may be reflected at the neural level (e.g., preserved neural responses in MST but altered responses in MT; Morrone et al. 2000).

The presence of face-selective responses in high-level visual regions in KL even before surgery contrasts with what was previously reported in MM, whose high-level visual cortex was unresponsive to faces when tested after sight restoration (Fine et al. 2003). Hence, while a total absence of visual input since an early age seems to permanently alter the functional response of high level face-selective regions (Fine et al. 2003; Röder et al. 2013), our findings suggest that even crude residual visual information may be sufficient in tuning face-selective regions to categorical information of faces at least. Supporting this assumption, electrophysiological studies in humans have shown larger amplitude on the N170/M170 for faces compared with nonface objects for low-pass filtered stimuli ($< \approx 2$ cpd) (Awasthi et al. 2013; Goffaux et al. 2003), and an fMRI study has demonstrated face-preferential responses over cars in the right FFA when using low-pass filtered stimuli (Gauthier et al. 2005). Here again, residual visual information provided by low spatial frequencies may have been sufficient to set the functional tuning of the face-selective network and allow basic face perception abilities such as accurate categorization even prior to surgery (Fig. 1*D*). Importantly, findings of face-selective responses in OFA and FFA even prior to surgery (Fig. 4 and Fig. 7*B*) do not necessarily imply that these regions are optimally tuned to individual face discrimination. In fact, KL's presurgical individual face discrimination (distinguishing between 2 different faces) was at chance level (Fig. 1, *E* and *F*). In the same vein, the presence of face-selective regions in the brain of acquired prosopagnosic patients is the neural signature of their ability to discriminate faces from nonface objects, despite profound deficits in individual face discrimination (Dricot et al. 2008; Rossion et al. 2003; Schiltz et al. 2006; Steeves et al. 2009). In these patients, however, the fMRI signal in these regions, despite being preferential for faces,

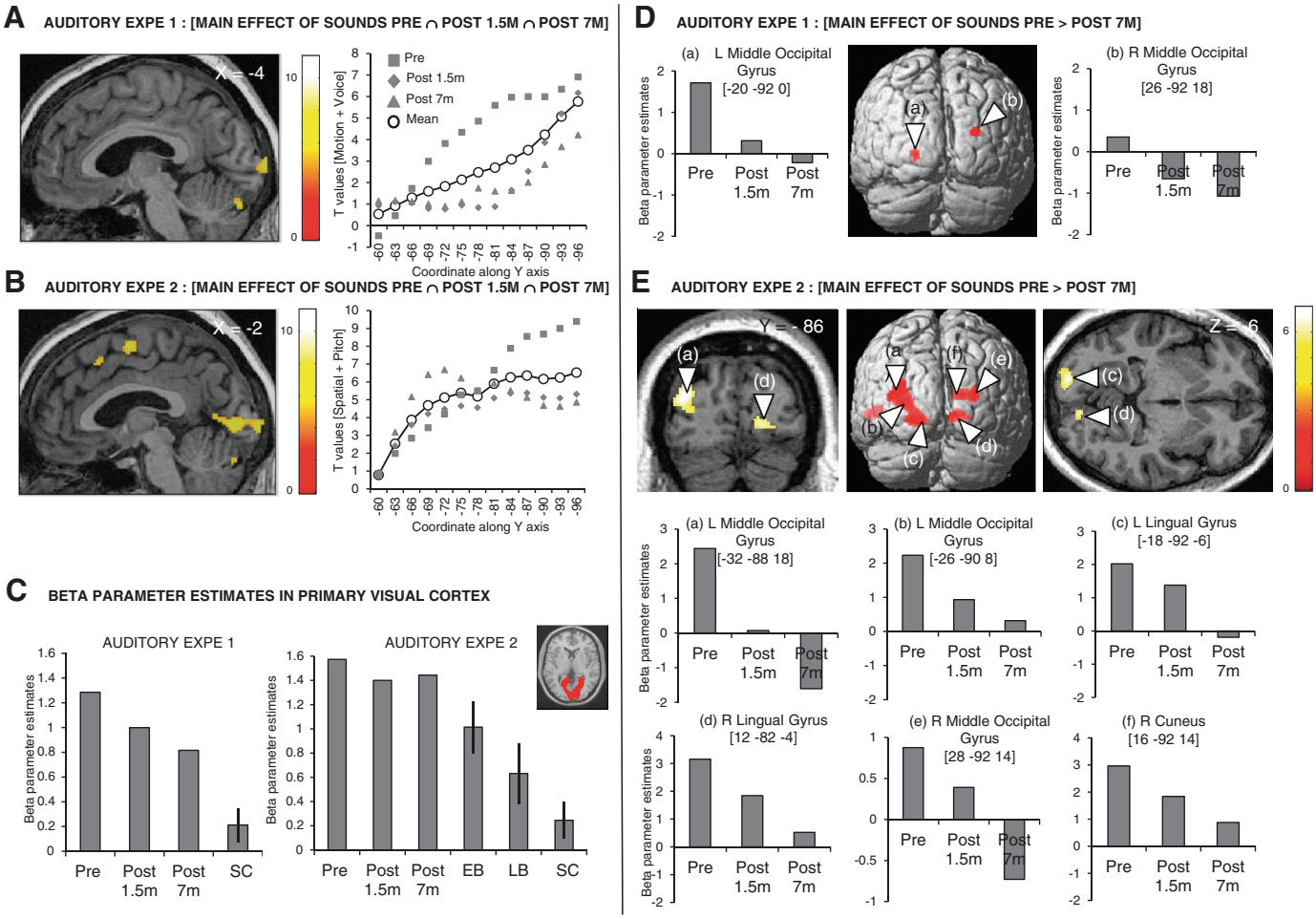

Fig. 5. fMRI activation maps of auditory processing. *A* and *B*: between-session conjunction analysis highlighting brain regions that are consistently activated during auditory stimulation across the 3 sessions in KL in *auditory experiment 1* ([Motion + Voice Pre ∩ Post 1.5m ∩ Post 7m], *A*) and *auditory experiment 2* ([Spatial + Pitch Pre ∩ Post 1.5m ∩ Post 7m], *B*). Corresponding *t* values are plotted along the calcarine sulcus from the most rostral pole (−60 in the *y*-axis) to the most caudal pole (−96 along the *y*-axis) for each session separately (Pre, Post 1.5m, and Post 7m) in gray and for the average of all sessions in black. *C*: beta parameter estimates are plotted for the main effect of sounds in an anatomical mask encompassing the pericalcarine region (primary visual cortex) in *auditory experiment 1* for KL (at Pre, Post 1.5m, and Post 7m) and sighted control subjects (SC) and in *auditory experiment 2* for KL (at Pre, Post 1.5m, and Post 7m), early blind (EB), late blind (LB), and sighted control (SC) subjects. Bars represent SE from the mean. *D* and *E*: brain regions showing larger recruitment during auditory stimulation at Pre relative to Post 7m in KL and associated beta parameter estimates in *auditory experiment 1* ([Motion + Voice × Pre > Post 7m], *D*) and *auditory experiment 2* ([Spatial + Pitch × Pre > Post 7m], *E*). Results are displayed at a threshold of $P < 0.05$ FWE corrected over the whole brain on sagittal, coronal, and transverse slices of KL's structural image normalized to MNI space.

does not show any evidence of sensitivity to the discrimination of individual faces (i.e., lack of release from adaptation with different compared with identical faces) (Dricot et al. 2008; Schiltz et al. 2006; Steeves et al. 2009). In KL, within-face discrimination abilities increased after surgery (Fig. 1, *E* and *F*) but no changes in activation were observed in face-selective regions (Fig. 4). Future studies with sight recovery individuals may therefore test sensitivity to faces in face-selective regions by means of adaptation paradigms to provide a finer investigation of neural responses to individual faces before and after surgery.

Presurgical Crossmodal Auditory Responses in Occipital Cortex and Overlap with Visual Responses

Our observation of auditory responses in the occipital cortex of an individual with residual preoperative vision (Fig. 5, *A–C*, Fig. 7, *C* and *D*) suggests that crossmodal reorganization can be observed even when the visual loss is not total and despite the presence of visual functional specialization in high-level visual cortex.

In the pericalcarine cortex, crossmodal responses were robust and reliable across both auditory experiments and sessions and were comparable to the responses measured in totally blind individuals (Fig. 5*C* and Fig. 7*D*). Remarkably, these responses in KL largely overlapped with visual responses in all sessions (Fig. 6). Findings of coexisting crossmodal and visual responses were previously reported within high-level visual cortex in two sight recovery subjects (Saenz et al. 2008) and in a case of severe visual impairment (Cheung et al. 2009). Our results thus extend these observations to the pericalcarine cortex, demonstrating that this region, classically considered as purely visual, can respond to both visual and auditory modalities in the instance of a life-long history of severely altered visual experience.

Across auditory experiments and sessions, estimated response amplitude during global sound processing steadily decreased from the most posterior part to the most anterior part of the calcarine sulcus (Fig. 5, *A* and *B*). In the sighted brain, the posterior part of the calcarine sulcus displays

Table 4. *Auditory experiment 1 fMRI results*

Area	Cluster Size	*x*, mm	*y*, mm	*z*, mm	*Z*	*P*
Conjunction [Motion + Voice Pre ∩ Post 1.5m ∩ Post 7m]						
L superior temporal gyrus	1,918	−64	−16	12	Inf	<0.001
R middle temporal gyrus	2,915	56	−22	−6	Inf	<0.001
R middle frontal gyrus	342	42	38	30	7.41	<0.001
R pericalcarine cortex	56	22	−94	−2	7.06	<0.001
L cerebellum	95	−4	−82	−24	6.61	<0.001
R inferior frontal gyrus	35	52	42	6	6.52	<0.001
R superior temporal gyrus	16	68	−38	22	6.25	<0.001
L pericalcarine cortex	104	−4	−102	6	6.10	<0.001
R superior temporal gyrus	37	40	4	−18	5.82	<0.001
L middle frontal gyrus	44	−38	52	10	5.77	<0.001
R superior frontal gyrus	55	6	6	66	5.37	0.002
R pericalcarine cortex	12	6	−92	12	5.34	0.003
L thalamus	14	−12	−16	6	5.33	0.003
R middle temporal gyrus	18	52	−48	8	5.22	0.005
L cerebellum	17	−22	−66	−22	5.20	0.005
R precentral gyrus	31	42	4	36	5.11	0.008
R supplementary motor area	16	8	16	50	5.09	0.009
[Motion + Voice Pre > Post 1.5m]						
No suprathreshold voxels						
[Motion + Voice Pre > Post 7m]						
R middle/superior occipital gyrus	18	26	−92	18	5.23	0.004
L middle occipital gyrus	16	−20	−92	0	4.91	0.020
[Motion + Voice Post 1.5m > Post 7m]						
No suprathreshold voxels						

Summary of the functional results obtained for the main effect of global sound processing in *auditory experiment 1* [Motion + Voice]. All coordinates reported in this table are significant after correction over the entire brain (FWE $P < 0.05$).

representations of the foveal and parafoveal visual field (Sereno et al. 1995) and contains neurons tuned to higher spatial frequencies (Singh et al. 2000). In line with KL's poor sensitivity to high spatial frequencies (Fig. 1*B*), we speculate that the reduced optical quality of her visual input since an early age prevented the normal development of populations of neurons in this region (Levin et al. 2010) and led this region to tune to auditory information (Cheung et al. 2009). These assumptions further raise the possibility that crossmodal responses interfere with visual functioning, preventing optimal visual recovery (as hypothesized in cochlear implant users for the recovery of auditory functions; see Buckley and Tobey 2011; Lee et al. 2007; Sandmann et al. 2012; Strelnikov et al. 2013).

The absence of consistent functional specialization in crossmodal responses across sessions (selective auditory activity for a specific task) within KL's visual cortex suggests that the nature of this crossmodal reorganization may differ from that observed in early-onset totally blind subjects (Collignon et al. 2011b) and rather resemble the reorganization observed in late-onset totally blind subjects (Collignon et al. 2013). Indeed, residual presurgical vision in KL has led to the development of visually specific responses in higher-level visual regions (Fig. 3*A* and Fig. 4), which in turn might have prevented the development of functionally specific crossmodal responses to auditory information. In the same vein, cortical visual areas such as hMT+/V5 do not display functionally specific crossmodal responses in late-onset blind individuals, presumably because developmental vision had tuned these regions to relevant visuo-spatial information before sight was lost (Bedny et al. 2010; Collignon et al. 2013). This assumption is in line with the "interactive specialization" principle of human postnatal brain development according to which the extent of plasticity observed within a given region after sensory deprivation is dependent on the degree of specialization already achieved by this region (Johnson 2011).

Table 5. *Auditory experiment 2 fMRI results*

Area	Cluster Size	*x*, mm	*y*, mm	*z*, mm	*Z*	*P*
Conjunction [Spatial + Pitch Pre ∩ Post 1.5m ∩ Post 7m]						
L postcentral gyrus	912	−58	−18	14	Inf	<0.001
R precentral gyrus	719	44	6	32	Inf	<0.001
R insula	260	32	22	6	Inf	<0.001
L inferior parietal lobule	2,393	−40	−44	42	Inf	<0.001
R inferior frontal gyrus	920	56	12	10	Inf	<0.001
L supplementary motor area	167	−8	−6	56	Inf	<0.001
R supramarginal gyrus	584	42	−40	36	Inf	<0.001
L inferior frontal gyrus	330	−50	8	12	Inf	<0.001
R superior frontal gyrus	329	8	20	44	7.43	<0.001
R pericalcarine	76	20	−96	0	7.16	<0.001
L superior occipital gyrus	732	−10	−102	6	7.13	<0.001
L cerebellum	118	−38	−60	−46	7.06	<0.001
R middle frontal gyrus	304	42	32	26	6.88	<0.001
R middle frontal gyrus		42	46	26	6.37	<0.001
L middle frontal gyrus	45	−34	52	12	6.71	<0.001
L superior parietal gyrus	143	−22	−70	50	6.55	<0.001
R superior occipital gyrus	17	16	−100	16	6.14	<0.001
L superior temporal gyrus	24	−42	−20	0	5.86	<0.001
R cerebellum	44	28	−50	−48	5.84	<0.001
L cerebellum	28	−12	−70	−46	5.82	<0.001
L insula	52	−34	22	−2	5.71	<0.001
L middle occipital gyrus	23	−30	−96	10	5.66	0.001
L inferior frontal gyrus	20	−34	34	14	5.59	0.001
L cerebellum	33	0	−82	−24	5.51	0.001
L lingual gyrus	20	−12	−78	−14	5.41	0.002
R cerebellum	20	16	−68	−46	5.41	0.002
L temporal pole	29	−56	14	−2	5.35	0.003
R superior frontal gyrus	14	24	2	62	5.23	0.006
L cerebellum	12	−18	−66	−24	5.22	0.006
[Spatial + Pitch Pre > Post 1.5m]						
No suprathreshold voxels						
[Spatial + Pitch Pre > Post 7m]						
L middle occipital gyrus	390	−32	−88	18	6.86	<0.001
L lingual gyrus		−18	−92	−6	6.21	<0.001
L middle occipital gyrus		−26	−90	8	5.79	<0.001
R lingual gyrus	69	12	−82	−4	6.33	<0.001
R superior frontal gyrus	96	20	0	70	6.19	<0.001
L superior temporal sulcus	96	−48	−28	2	6.05	<0.001
R middle/sup occipital gyrus	95	28	−92	14	6.02	<0.001
R cuneus/middle occipital gyrus		16	−92	14	5.96	<0.001
[Spatial + Pitch Post 1.5m > Post 7m]						
R inferior occipital gyrus	84	46	−82	−4	6.35	<0.001
R middle occipital gyrus	43	40	−76	4	5.49	0.001
R middle frontal gyrus	28	4	36	−16	5.41	0.002
L middle temporal gyrus	15	−54	−34	0	5.14	0.009

Summary of the functional results obtained for the main effect of global sound processing in *auditory experiment 2* [Spatial + Pitch]. All coordinates reported in this table are significant after correction over the entire brain (FWE $P < 0.05$).

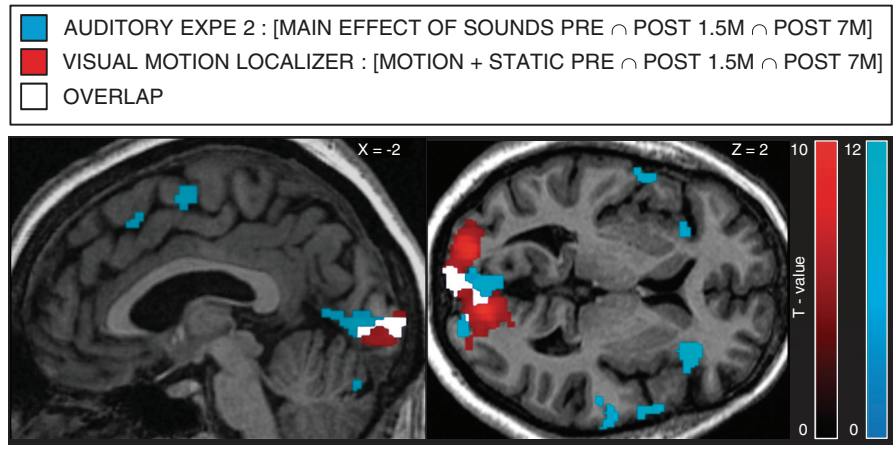

Fig. 6. Overlap between auditory and visual responses in KL's primary visual cortex in all sessions. Shown in blue is the between-session conjunction of the main effect of auditory conditions in *auditory experiment 2* ([Spatial + Pitch Pre ∩ Post 1.5m ∩ Post 7m]). Shown in red is the between-session conjunction of the main effect of visual conditions in the Motion localizer ([Motion + Static Pre ∩ Post 1.5m ∩ Post 7m]). Shown in white is the overlap. Results are displayed at a threshold of $P < 0.05$ FWE corrected over the whole brain on sagittal and transverse slices of KL's structural image normalized to MNI space.

Postsurgical Decrease in Crossmodal Auditory Responses in Extrastriate Occipital Cortex

In contrast to what was observed in pericalcarine regions, some extrastriate occipital regions displayed robust between-session decreases in crossmodal recruitment in both auditory experiments. Several regions showing robust auditory activation before surgery even showed sound-related deactivation 7 mo after sight-restoration (Fig. 5, *D* and *E*), as typically observed in sighted individuals (Laurienti et al. 2002). Therefore, the progressive appearance of sound-related deactivations in KL's extrastriate occipital cortex may parallel the recovery of visual tuning observed within these regions (Fig. 3*B*). Overall, our results suggest that the primary visual cortex maintains its involvement in the processing of nonvisual information despite sight restoration, whereas presurgical auditory responses in extrastriate regions decrease after sight restora-

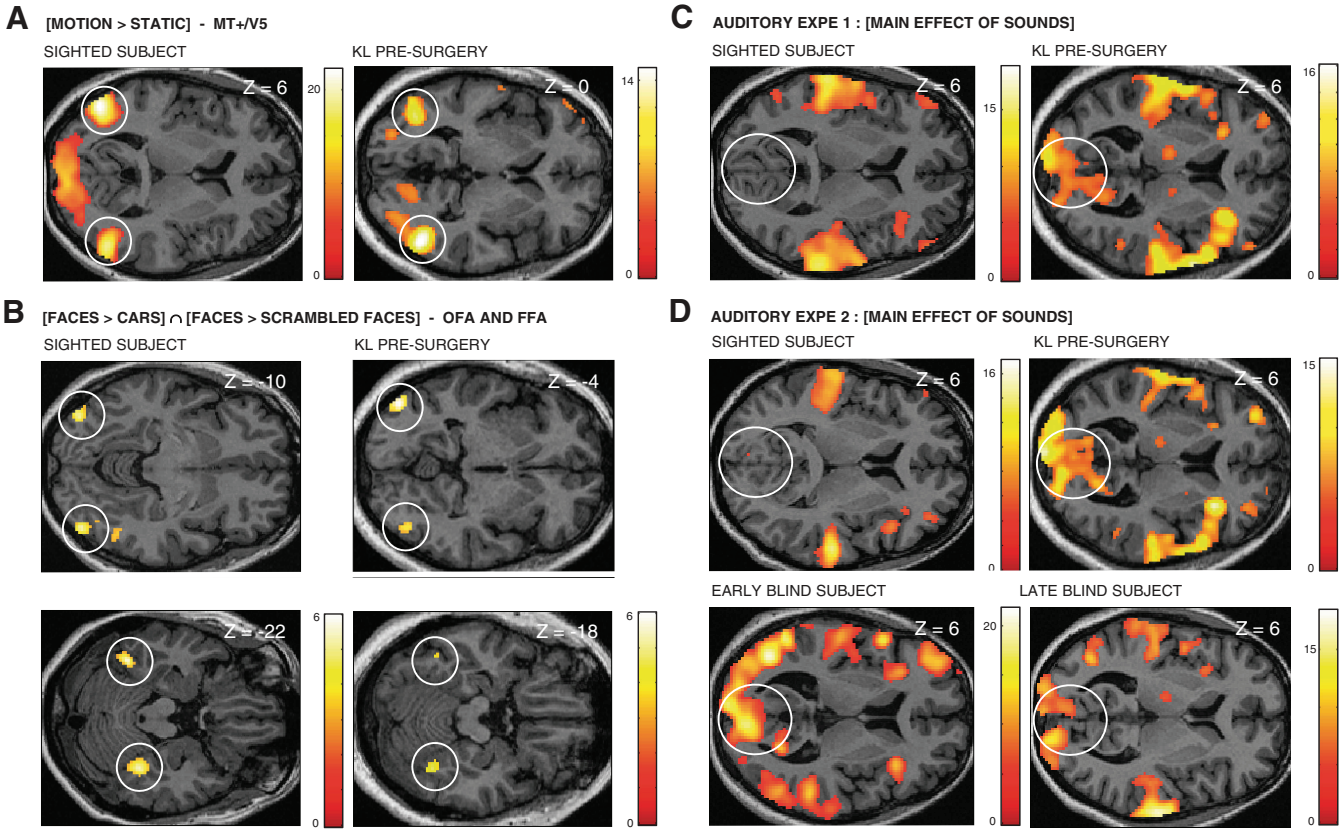

Fig. 7. fMRI activation maps in control subjects. *A* and *B*: brain regions responding more to moving relative to stationary dots (*A*) and Faces relative to both Cars and Scrambled Faces (*B*) are shown in a representative subject from the sighted control group (right-handed woman, 32 yr old) and in KL before surgery. *C*: brain regions responding during global sound processing in *auditory experiment 1* ([Motion + Voice]) are shown in a representative subject from the sighted control group (right-handed woman, 32 yr old) and KL before surgery. *D*: brain regions responding during global sound processing in *auditory experiment 2* ([Spatial + Pitch]) are shown in a representative subject from the sighted control group (right-handed woman, 48 yr old), a representative subject from the early-blind group (right-handed woman, 56 yr old), a representative subject from the late-blind group (right-handed woman, 46 yr old), and KL before surgery. Results are displayed at a threshold $P < 0.05$ corrected (FWE) over the whole brain in *A*, *C*, and *D* and at a threshold of $P < 0.001$ uncorrected in *B* on transverse slices of each subject's structural image normalized to MNI space.

tion. Taken together, these data compellingly demonstrate the existence of region-specific mechanisms in the way visual deprivation and restoration affect the modality tuning of the occipital cortex.

Postsurgical Increase in Gray Matter Density

As early as 1.5 mo after surgery, significant increases in gray matter density were evidenced in several portions of the low-level visual cortex (Fig. 2*C*). Fast experience-dependent gray matter density increases have been previously reported in longitudinal studies involving training protocols such as complex sensorimotor tasks (Draganski et al. 2004; Taubert et al. 2010), mirror reading (Ilg et al. 2008), and visual perceptual learning (Ditye et al. 2013). Findings from the present study demonstrate that important structural changes may be induced far more quickly than previously expected (gains of >8% in gray matter density in occipital cortex after only 1.5 mo) when significantly increasing the quality of a sensory input (here, vision). Although the cellular correlates of macrostructural changes evidenced in human neuroimaging remain elusive, rapid structural changes associated with sensory experience in adulthood have been mainly related to mechanisms acting at the neural level (including remodeling of dendritic spines, synaptogenesis, and synapse elimination) and mechanisms involving nonneuronal glial cells (gliogenesis) (Zatorre et al. 2012), both of which have been documented in mice after both sensory deprivation and restoration (Tremblay et al. 2010; Zuo et al. 2005).

Conclusions

The occipital cortex has long served as a front-runner model to understand how brain regions develop, specialize, and reorganize their tuning toward a specific input and function (Hubel 1995). We provide the first longitudinal investigation of how crossmodal plasticity interacts with restored vision in a sight recovery subject. We show that structural and functional reorganization of occipital regions are present in an individual with a long-standing history of severe visual impairment and that such reorganizations can be partially reversed by visual restoration in adulthood.

ACKNOWLEDGMENTS

We are grateful to KL for her inexhaustible patience and motivation during the project. We thank Jorge Jovicich and Domenico Zacà for their help on the structural data analyses and Pascal Belin for providing the tools for sound scrambling.

GRANTS

This work was supported by the Canada Research Chair Program (F. Lepore), the Canadian Institutes of Health Research (F. Lepore, G. Albouy), the Saint-Justine Foundation (O. Collignon), the European Research Council (starting grant MADVIS, ERC-StG 337573, O. Collignon), the Veronneau Troutman Foundation (G. Dormal), the Fonds de Recherche en Ophtalmologie de l'Université de Montréal (FROUM) (G. Dormal, M. Harissi-Dagher), PAI/UIAP Grant PAI/33 (B. Rossion), and the Belgian National Fund for Scientific Research (G. Dormal, O. Collignon, and B. Rossion).

DISCLOSURES

No conflicts of interest, financial or otherwise, are declared by the author(s).

AUTHOR CONTRIBUTIONS

Author contributions: G.D., F.L., M.H.-D., G.A., A.B., B.R., and O.C. conception and design of research; G.D. and O.C. performed experiments; G.D., G.A., A.B., and O.C. analyzed data; G.D., F.L., G.A., B.R., and O.C. interpreted results of experiments; G.D. and O.C. prepared figures; G.D. and O.C. drafted manuscript; G.D., F.L., M.H.-D., G.A., A.B., B.R., and O.C. edited and revised manuscript; G.D., F.L., M.H.-D., G.A., A.B., B.R., and O.C. approved final version of manuscript.

REFERENCES

Ackroyd C, Humphrey NK, Warrington EK. Lasting effects of early blindness. A case study. *Q J Exp Psychol* 26: 114–124, 1974.

Aksoy M, Forman C, Straka M, Çukur T, Hornegger J, Bammer R. Hybrid prospective and retrospective head motion correction to mitigate cross-calibration errors. *Magn Reson Med* 67: 1237–1251, 2012.

Aldave AJ, Kamal KM, Vo RC, Yu F. The Boston type I keratoprosthesis: improving outcomes and expanding indications. *Ophthalmology* 116: 640–651, 2009.

Amedi A, Floel A, Knecht S, Zohary E, Cohen LG. Transcranial magnetic stimulation of the occipital pole interferes with verbal processing in blind subjects. *Nat Neurosci* 7: 1266–1270, 2004.

Amedi A, Raz N, Pianka P, Malach R, Zohary E. Early "visual" cortex activation correlates with superior verbal memory performance in the blind. *Nat Neurosci* 6: 758–766, 2003.

Awasthi B, Sowman PF, Friedman J, Williams MA. Distinct spatial scale sensitivities for early categorization of faces and places: neuromagnetic and behavioral findings. *Front Hum Neurosci* 7: 91, 2013.

Bavelier D, Neville HJ. Cross-modal plasticity: where and how? *Nat Rev Neurosci* 3: 443–452, 2002.

Bedny M, Konkle T, Pelphrey K, Saxe R, Pascual-Leone A. Sensitive period for a multimodal response in human visual motion area MT/MST. *Curr Biol* 20: 1900–1906, 2010.

Belin P, Zatorre RJ, Lafaille P, Ahad P, Pike B. Voice-selective areas in human auditory cortex. *Nature* 403: 309–312, 2000.

Brett M, Anton JL, Valabregue R, Poline JB. Region of interest analysis using the MarsBar toolbox for SPM 99. *Neuroimage* 16: S497, 2002.

Buckley KA, Tobey EA. Cross-modal plasticity and speech perception in pre- and postlingually deaf cochlear implant users. *Ear Hear* 32: 2–15, 2011.

Carlson S, Hyvärinen L, Raninen A. Persistent behavioural blindness after early visual deprivation and active visual rehabilitation: a case report. *Br J Ophthalmol* 70: 607–611, 1986.

Cheung SH, Fang F, He S, Legge GE. Retinotopically specific reorganization of visual cortex for tactile pattern recognition. *Curr Biol* 19: 596–601, 2009.

Cohen LG, Celnik P, Pascual-Leone A, Corwell B, Falz L, Dambrosia J, Honda M, Sadato N, Gerloff C, Catalá MD, Hallett M. Functional relevance of cross-modal plasticity in blind humans. *Nature* 389: 180–183, 1997.

Collignon O, Champoux F, Voss P, Lepore F. Sensory rehabilitation in the plastic brain. *Prog Brain Res* 191: 211–231, 2011a.

Collignon O, Dormal G, Albouy G, Vandewalle G, Voss P, Phillips C, Lepore F. Impact of blindness onset on the functional organization and the connectivity of the occipital cortex. *Brain* 136: 2769–2783, 2013.

Collignon O, Lassonde M, Lepore F, Bastien D, Veraart C. Functional cerebral reorganization for auditory spatial processing and auditory substitution of vision in early blind subjects. *Cereb Cortex* 17: 457–465, 2007.

Collignon O, Vandewalle G, Voss P, Albouy G, Charbonneau G, Lassonde M, Lepore F. Functional specialization for auditory-spatial processing in the occipital cortex of congenitally blind humans. *Proc Natl Acad Sci USA* 108: 4435–4440, 2011b.

Crawford JR, Garthwaite PH, Porter S. Point and interval estimates of effect sizes for the case-controls design in neuropsychology: rationale, methods, implementations, and proposed reporting standards. *Cogn Neuropsychol* 27: 245–260, 2010.

Ditye T, Kanai R, Bahrami B, Muggleton NG, Rees G, Walsh V. Rapid changes in brain structure predict improvements induced by perceptual learning. *Neuroimage* 81: 205–212, 2013.

Dormal G, Collignon O. Functional selectivity in sensory-deprived cortices. *J Neurophysiol* 105: 2627–2630, 2011.

Dormal V, Andres M, Dormal G, Pesenti M. Mode-dependent and mode-independent representations of numerosity in the right intraparietal sulcus. *Neuroimage* 52: 1677–1686, 2010.

Draganski B, Gaser C, Busch V, Schuierer G, Bogdahn U, May A. Neuroplasticity: changes in grey matter induced by training. *Nature* 427: 311–312, 2004.

Dricot L, Sorger B, Schiltz C, Goebel R, Rossion B. The roles of "face" and "non-face" areas during individual face perception: evidence by fMRI adaptation in a brain-damaged prosopagnosic patient. *Neuroimage* 40: 318–332, 2008.

Fine I, Wade AR, Brewer AA, May MG, Goodman DF, Boynton GM, Wandell BA, MacLeod DI. Long-term deprivation affects visual perception and cortex. *Nat Neurosci* 6: 915–916, 2003.

Gauthier I, Curby KM, Skudlarski P, Epstein RA. Individual differences in FFA activity suggest independent processing at different spatial scales. *Cogn Affect Behav Neurosci* 5: 222–234, 2005.

Goffaux V, Gauthier I, Rossion B. Spatial scale contribution to early visual differences between face and object processing. *Brain Res Cogn Brain Res* 16: 416–424, 2003.

Gougoux F, Belin P, Voss P, Lepore F, Lassonde M, Zatorre RJ. Voice perception in blind persons: a functional magnetic resonance imaging study. *Neuropsychologia* 47: 2967–2974, 2009.

Gougoux F, Zatorre RJ, Lassonde M, Voss P, Lepore F. A functional neuroimaging study of sound localization: visual cortex activity predicts performance in early-blind individuals. *PLoS Biol* 3: e27, 2005.

Gregory RL, Wallace JG. Recovery from early blindness. In: *Concepts and Mechanisms of Perception*, edited by Gregory RL. London: Duckworth, 1974.

Harvey LO. Efficient estimation of sensory thresholds with ML-PEST. *Spat Vis* 11: 121–128, 1997.

Haxby J, Hoffman E, Gobbini M. The distributed human neural system for face perception. *Trends Cogn Sci* 4: 223–233, 2000.

Heimler B, Weisz N, Collignon O. Revisiting the adaptive and maladaptive effects of crossmodal plasticity. *Neuroscience* 283: 44–63, 2014.

Hubel DH. *Eye, Brain, Vision*. New York: Scientific American Library/Scientific American Books, 1995.

Ilg R, Wohlschläger AM, Gaser C, Liebau Y, Dauner R, Wöller A, Zimmer C, Zihl J, Mühlau M. Gray matter increase induced by practice correlates with task-specific activation: a combined functional and morphometric magnetic resonance imaging study. *J Neurosci* 28: 4210–4215, 2008.

Johnson MH. Interactive specialization: a domain-general framework for human functional brain development? *Dev Cogn Neurosci* 1: 7–21, 2011.

Khan BF, Harissi-Dagher M, Khan DM, Dohlman CH. Advances in Boston keratoprosthesis: enhancing retention and prevention of infection and inflammation. *Int Ophthalmol Clin* 47: 61–71, 2007.

Laurienti PJ, Burdette JH, Wallace MT, Yen YF, Field AS, Stein BE. Deactivation of sensory-specific cortex by cross-modal stimuli. *J Cogn Neurosci* 14: 420–429, 2002.

Lee HJ, Giraud AL, Kang E, Oh SH, Kang H, Kim CS, Lee DS. Cortical activity at rest predicts cochlear implantation outcome. *Cereb Cortex* 17: 909–917, 2007.

Levin N, Dumoulin SO, Winawer J, Dougherty RF, Wandell BA. Cortical maps and white matter tracts following long period of visual deprivation and retinal image restoration. *Neuron* 65: 21–31, 2010.

Maclaren J, Herbst M, Speck O, Zaitsev M. Prospective motion correction in brain imaging: a review. *Magn Reson Med* 69: 621–636, 2013.

Mahon BZ, Anzellotti S, Schwarzbach J, Zampini M, Caramazza A. Category-specific organization in the human brain does not require visual experience. *Neuron* 63: 397–405, 2009.

Maldjian JA, Laurienti PJ, Kraft RA, Burdette JH. An automated method for neuroanatomic and cytoarchitectonic atlas-based interrogation of fMRI data sets. *Neuroimage* 19: 1233–1239, 2003.

Maunsell JH, Nealey TA, DePriest DD. Magnocellular and parvocellular contributions to responses in the middle temporal visual area (MT) of the macaque monkey. *J Neurosci* 10: 3323–3334, 1990.

Merabet LB, Pascual-Leone A. Neural reorganization following sensory loss: the opportunity of change. *Nat Rev Neurosci* 11: 44–52, 2009.

Morrone MC, Tosetti M, Montanaro D, Fiorentini A. A cortical area that responds specifically to optic flow, revealed by fMRI. *Nat Neurosci* 3: 1322–1328, 2000.

Newsome WT, Paré EB. A selective impairment of motion perception following lesions of the middle temporal visual area (MT). *J Neurosci* 8: 2201–2211, 1988.

Noppeney U. The effects of visual deprivation on functional and structural organization of the human brain. *Neurosci Biobehav Rev* 31: 1169–1180, 2007.

Reich L, Szwed M, Cohen L, Amedi A. A ventral visual stream reading center independent of visual experience. *Curr Biol* 21: 363–368, 2011.

Ricciardi E, Pietrini P. New light from the dark: what blindness can teach us about brain function. *Curr Opin Neurol* 24: 357–363, 2011.

Robert MC, Harissi-Dagher M. Boston type 1 keratoprosthesis: the CHUM experience. *Can J Ophthalmol* 46: 164–168, 2011.

Röder B, Ley P, Shenoy BH, Kekunnaya R, Bottari D. Sensitive periods for the functional specialization of the neural system for human face processing. *Proc Natl Acad Sci USA* 110: 16760–16765, 2013.

Rossion B. Picture-plane inversion leads to qualitative changes of face perception. *Acta Psychol* 128: 274–289, 2008.

Rossion B, Caldara R, Seghier M, Schuller AM, Lazeyras F, Mayer E. A network of occipito-temporal face-sensitive areas besides the right middle fusiform gyrus is necessary for normal face processing. *Brain* 126: 2381–2395, 2003.

Rossion B, Hanseeuw B, Dricot L. Defining face perception areas in the human brain: a large-scale factorial fMRI face localizer analysis. *Brain Cogn* 79: 138–157, 2012.

Sadr J, Sinha P. Object recognition and Random Image Structure Evolution. *Cogn Sci* 28: 259–287, 2004.

Saenz M, Lewis LB, Huth AG, Fine I, Koch C. Visual motion area MT+/V5 responds to auditory motion in human sight-recovery subjects. *J Neurosci* 28: 5141–5148, 2008.

Sandmann P, Dillier N, Eichele T, Meyer M, Kegel A, Pascual-Marqui RD, Marcar VL, Jäncke L, Debener S. Visual activation of auditory cortex reflects maladaptive plasticity in cochlear implant users. *Brain* 135: 555–568, 2012.

Schiltz C, Sorger B, Caldara R, Ahmed F, Mayer E, Goebel R, Rossion B. Impaired face discrimination in acquired prosopagnosia is associated with abnormal response to individual faces in the right middle fusiform gyrus. *Cereb Cortex* 16: 574–586, 2006.

Schulz J, Siegert T, Reimer E, Labadie C, Maclaren J, Herbst M, Zaitsev M, Turner R. An embedded optical tracking system for motion-corrected magnetic resonance imaging at 7T. *MAGMA* 25: 443–453, 2012.

Sereno MI, Dale AM, Reppas JB, Kwong KK, Belliveau JW, Brady TJ, Rosen BR, Tootell RB. Borders of multiple visual areas in humans revealed by functional magnetic resonance imaging. *Science* 268: 889–893, 1995.

Singh KD, Smith AT, Greenlee MW. Spatiotemporal frequency and direction sensitivities of human visual areas measured using fMRI. *Neuroimage* 12: 550–564, 2000.

Steeves J, Dricot L, Goltz HC, Sorger B, Peters J, Milner AD, Goodale MA, Goebel R, Rossion B. Abnormal face identity coding in the middle fusiform gyrus of two brain-damaged prosopagnosic patients. *Neuropsychologia* 47: 2584–2592, 2009.

Strelnikov K, Rouger J, Demonet JF, Lagleyre S, Fraysse B, Deguine O, Barone P. Visual activity predicts auditory recovery from deafness after adult cochlear implantation. *Brain* 136: 3682–3695, 2013.

Sunaert S, Van Hecke P, Marchal G, Orban GA. Motion-responsive regions of the human brain. *Exp Brain Res* 127: 355–370, 1999.

Taubert M, Draganski B, Anwander A, Müller K, Horstmann A, Villringer A, Ragert P. Dynamic properties of human brain structure: learning-related changes in cortical areas and associated fiber connections. *J Neurosci* 30: 11670–11677, 2010.

Tootell RB, Devaney KJ, Young JC, Postelnicu G, Rajimehr R, Ungerleider LG. fMRI mapping of a morphed continuum of 3D shapes within inferior temporal cortex. *Proc Natl Acad Sci USA* 105: 3605–3609, 2008.

Tootell RB, Reppas JB, Kwong KK, Malach R, Born RT, Brady TJ, Rosen BR, Belliveau JW. Functional analysis of human MT and related visual cortical areas using magnetic resonance imaging. *J Neurosci* 15: 3215–3230, 1995.

Tremblay MÈ, Lowery RL, Majewska AK. Microglial interactions with synapses are modulated by visual experience. *PLoS Biol* 8: e1000527, 2010.

Tzourio-Mazoyer N, Landeau B, Papathanassiou D, Crivello F, Etard O, Delcroix N, Mazoyer B, Joliot M. Automated anatomical labeling of activations in SPM using a macroscopic anatomical parcellation of the MNI MRI single-subject brain. *Neuroimage* 15: 273–289, 2002.

Willenbockel V, Sadr J, Fiset D, Horne GO, Gosselin F, Tanaka JW. Controlling low-level image properties: the SHINE toolbox. *Behav Res Methods* 42: 671–684, 2010.

Zatorre RJ, Fields RD, Johansen-Berg H. Plasticity in gray and white: neuroimaging changes in brain structure during learning. *Nat Neurosci* 15: 528–536, 2012.

Zuo Y, Yang G, Kwon E, Gan WB. Long-term sensory deprivation prevents dendritic spine loss in primary somatosensory cortex. *Nature* 436: 261–265, 2005.